



# Summary report of tested materials

D1.4

# RecHycle

Oct 2024



Centre National de la Recherche Scientifique



## Document Information

<b>Project Title</b>	Recycling (renewable) hydrogen for climate neutrality		
<b>Acronym</b>	Rechycle		
<b>Grant agreement no.</b>	101058692		
<b>Topic ID</b>	HORIZON-CL4-2021-TWIN-TRANSITION-01		
<b>EU Contribution</b>	€ 6,226,743.00		
<b>Coordinating entity</b>	ArcelorMittal Belgium		
<b>Start date</b>	01 Jun 2022	<b>End date</b>	31 Nov 2026
<b>Deliverable</b>	1.4	<b>WP</b>	1
<b>Deliverable type</b>	R	<b>Dissemination level</b>	PU
<b>Lead beneficiary</b>	JOA		
<b>Authors</b>	Dr DI Vojislav Petrovic-Filipovic, M.Sc. Katharina Shickle		
<b>Contributions from</b>	Yann Graz		
<b>Approved</b>	Vojislav Petrovic-Filipovic		

**Disclaimer:** This document and its content reflect only the author's view; therefore, the European Commission is not responsible for any use that may be made of the information it contains.

### Change Records

<b>Version</b>	<b>Date</b>	<b>Changes</b>
Version 1	26.04.2024	Draft of the report generated
Version 2	20.05.2024	Pre-final version generated
Version 3	29.05.2024	Final version generated

## Project Summary

RecHycle's goal is to implement a gas hub capable of mixing metallurgic gases produced on-site with or without external (green) hydrogen sources. This will ultimately be fed into the Blast Furnace and a future DRI furnace to produce green steel sustainably. The project will demonstrate a cost-efficient solution to decrease carbon emissions by initiating a new industrial symbiosis between and within the steel and chemical industries and renewable energy sources (e.g. wind or solar to obtain green electricity or hydrogen). The project will contribute to the shift towards a circular economy where waste products are valorised to the maximum of their potential. Furthermore, the project will serve as a stepping stone towards further developing synergies between companies within the North Sea Port industrial area, thus creating new opportunities for innovation and economic activities. Challenges to be addressed are the dynamic optimisation of gas mixtures and flows, minimising risks of hydrogen on material embrittlement, ceramic feed-inlet (Tuyeres) within the furnaces, the quality of the produced steel and the (future) material scrap streams of the DRI. RecHycle will be executed through a consortium of 6 partners from 4 different countries, including 1 industrial partner that is world-leading in the steel manufacturing industry and 5 research partners specialised in hydrogen-based studies.

**Acknowledgement:** RecHycle - Recycling renewable hydrogen for climate neutrality (grant agreement number: 101058692) is funded under the call HORIZON-CL4-2021-TWIN-TRANSITION-01-22 within Horizon Europe, the European Union's framework programme for research and innovation.

## RecHycle Consortium

The following table contains information about the consortium members.

Name	Country	Contact
ArcelorMittal Belgium  ArcelorMittal	Belgium	<b>Project Coordinator:</b> Joke Bauwens Joke.bauwens@arcelormittal.com
Joanneum Research Forschungsgesellschaft  JOANNEUM RESEARCH	Austria	<b>Participant:</b> Vojislav Petrovic vojislav.petrovic@joanneum.at
Università Politecnica delle Marche  UNIVERSITÀ POLITECNICA DELLE MARCHE	Italy	<b>Participant:</b> Filippo E. Ciarapica f.e.ciarapica@univpm.it
ArcelorMittal Maizières Research  ArcelorMittal	France	<b>Participant:</b> Rodolfo Santos Ferreira rodolfopaulo.santosferreira@arcelormittal.com
Centre National de la Recherche Scientifique (CNRS)  Centre National de la Recherche Scientifique	France	<b>Participant:</b> Gerard Vignoles vinhola@lcts.u-bordeaux.fr
IRT Saint Exupéry  IRT SAINT EXUPÉRY	France	<b>Participant:</b> Laurent Ferres laurent.ferres@irt-saintexupery.com

## Table of Contents

<b>1</b>	<b>Executive Summary .....</b>	<b>10</b>
<b>2</b>	<b>Definition of the purpose of the study .....</b>	<b>11</b>
<b>3</b>	<b>Definition of the work methodology .....</b>	<b>12</b>
<b>4</b>	<b>Definition of the material and methods.....</b>	<b>13</b>
<b>5</b>	<b>Results and discussion .....</b>	<b>18</b>
<b>6</b>	<b>Conclusions and future work.....</b>	<b>40</b>

## List of Figures

Figure 1. The mechanism of Hydrogen infiltration. ....	11
Figure 2. Hydrogenisation (H <sub>2</sub> -O) setup (left) and the sample holder (right).....	15
Figure 3. Mini FP2 testing equipment.....	17
Figure 4. TESCAN's SEM equipment. ....	18
Figure 5: The microstructure overview of the as-received Material 1 pipe of Arcelor Mittal (left) and the Material 1 plate from Good Fellow (right) .....	19
Figure 6: The microstructure of the as-received Material 1 plate depicting the pores and cavities at the surface.....	19
Figure 7: The microstructure of the as-received Material 1 plate depicting the pores and cavities from the cross section of the material.....	20
Figure 8: Haynes Alloy from Good Fellow Rod (left) vs. the Material 2 pipe from Arcelor Mittal (right)	20
<i>Figure 9: Wöhlercurve of Material 1 Alloy uncharged vs. Material 1 Alloy 48h charged at RT vs charged at HT.....</i>	<i>23</i>
Figure 10. Wöhler curve of uncharged, RT charged and HT charged Material 2 alloy specimens, with the potential curves extrapolated upon the raw data. ....	26
Figure 11: The microstructure of the 48 h RT hydrogen charged Material 1 plate depicting the pores and cavities from the cross section of the material. Left: Microstructure does not change, No evident hydrides or other formations between the grains. Right: Crack that formed through fatigue testing.....	29
Figure 12: SEM images of different sections/samples to show the absence of the Hydrogen induced cracks and microstructural changes in RT charged samples.....	30
Figure 13: SEM images of different sections/samples to show the absence of the Hydrogen induced cracks and microstructural changes in HT charged samples (Sample 1).....	31
Figure 14: SEM images of different sections/samples to show the absence of the Hydrogen induced cracks and microstructural changes in HT charged samples (Sample 2).....	32
Figure 15. Microstructural analysis of the Material 2, sample 1 – left charged at RT, right uncharged, three different sections. ....	33
Figure 16. Microstructural analysis of the Material 2, sample 1 – left charged at HT, right uncharged, three different sections. ....	34
Figure 17: Fracture surfaces of Material 1 uncharged (right) vs. Material 1 charged at room temperature (left) outer region of sample.....	35
Figure 18: Fracture surfaces of Material 1 uncharged (right) vs. Material 1 charged at room temperature (left) outer region of sample.....	35
Figure 19: Fracture surfaces of Material 1 uncharged (right) vs. Material 1 charged at room temperature (left) inner region of sample.....	36
Figure 20: Fracture surfaces of Material 1 uncharged (right) vs. Material 1 charged at high temperature (left) outer region of sample.....	36
Figure 21: Fracture surfaces of Material 1 uncharged (right) vs. Material 1 charged at high temperature (left) outer region of sample.....	37

Figure 22: Fracture surfaces of Material 1 uncharged (right) vs. Material 1 charged at high temperature (left) inner region of sample..... 37

Figure 23: Fracture surfaces of Material 2 uncharged (left) vs. Material 2 charged at room temperature (right) inner region of sample..... 38

Figure 24: Fracture surfaces of Material 2 uncharged (left) vs. Material 2 charged at room temperature (right) region of crack initiation of sample..... 38

Figure 25: Fracture surfaces of Haynes uncharged (left) vs. Material 2 charged at room temperature (right) outer region of sample ..... 39

Figure 26: Fracture surfaces of Material 2 uncharged (left) vs. Material 2 charged at high temperature (right) inner region of sample..... 39

Figure 27: Fracture surfaces of Material 2 uncharged (left) vs. Material 2 charged at high temperature (right) region of crack initiation of sample..... 40

Figure 28:Fracture surfaces of Haynes uncharged (left) vs. Material 2 charged at high temperature (right) outer region of sample..... 40

## List of Tables

Table 1. The chemical composition of the materials .....	13
Table 2: Calculated number of cycles at pre-defined max. stress according to the power fit of the uncharged Material 1 Alloy .....	23
Table 3: Calculated number of cycles at pre-defined max. stress according to the power fit of the RT charged Material 1 Alloy; The resulting HE factor with and without the correction through the statistical error of the machine .....	23
Table 4: Calculated number of cycles at pre-defined max. stress according to the power fit of the HT charged Material 1 Alloy; The resulting HE factor with and without the correction through the statistical error of the machine .....	24
Table 5. Sample dimensions, number of cycles at 40% and 90% respectively and the maximum stress applied - uncharged.....	24
Table 6. Sample dimensions, number of cycles at $N_{40\%}$ and $N_{90\%}$ respectively and the maximum stress applied – charged at RT for 48h.....	24
Table 7: Sample dimensions, number of cycles at $N_{40\%}$ and $N_{90\%}$ respectively and the maximum stress applied – charged at HT for 48h.....	25
Table 8: Calculated number of cycles at pre-defined max. stress according to the power fit of the uncharged Material 2 Alloy .....	26
Table 9: Calculated number of cycles at pre-defined max. stress according to the power fit of the RT charged Material 2 Alloy; The resulting HE factor with and without the correction through the statistical error of the machine .....	26
Table 10: Calculated number of cycles at pre-defined max. stress according to the power fit of the HT charged Material 2 Alloy; The resulting HE factor with and without the correction through the statistical error of the machine .....	27
Table 11. Sample dimensions, number of cycles at $N_{40\%}$ and $N_{90\%}$ respectively and the maximum stress applied – uncharged.....	27
Table 12. Sample dimensions, number of cycles at $N_{40\%}$ and $N_{90\%}$ respectively and the maximum stress applied – charged at RT for 48h.....	27
Table 13. Sample dimensions, number of cycles at $N_{40\%}$ and $N_{90\%}$ respectively and the maximum stress applied – charged at HT for 48h.....	28
Table 14: Atomic weight percentage of the uncharged, RT and HT Material 1 Alloy; Sample 3.2 .....	28
Table 15: Mass weight percentage of the uncharged, RT and HT Material 2; Sample 1 .....	32
Table 16: Atomic weight percentage of the uncharged, RT and HT Material 2; Sample 2.....	32

# 1 Executive Summary

In this report, a summary of the material testing by exposure on Hydrogen in different conditions will be presented. The report is structured in the following way:

- Definition of the purpose of the study contained in the report;
- Definition of the methodology of work, including the strategy of the material testing and the evaluation of the results;
- Definition of the material and methods;
- Presentation of the results, and
- Discussion of the results, drawing of the main conclusion of this report and proposition of the future work.

## 2 Definition of the purpose of the study

The transition of the European industry to the green energy sources is driving many different research and innovation works, which are mainly focussed on the change in the main energy sources in the industrial processes. One of the most interesting, due to its positive effect on the carbon footprint, is Hydrogen as a combustion fuel. It is a fuel not exempt from challenges – when it comes to the use in transport (effects like flame attachment or flashback are still challenging<sup>1</sup>), but it represents the most promising alternative to the fossil fuels, especially for the use in the industrial facilities such as steelmaking industry.

However, there are relevant material challenges related to the use of Hydrogen in metallic components. Hydrogen is a very volatile and reactive gas. In contact with the material, it makes mostly two possible reactions – either it infiltrates and positions at the border of the grains, using the opportunity to accumulate, expand and promote cracks<sup>2</sup>, or it reacts with the metallic material and creates brittle formation, mostly hydrides<sup>3</sup>. In both cases, the related phenomena cause fragilization, commonly known as Hydrogen Embrittlement (HE). Figure 1 shows the mechanism of HE. This is a detrimental effect, which leads to the weakening of the material and premature failure. In the installations, such as hydrogen-driven steel making this would be a severe event, since Hydrogen is very flammable and could cause tragic explosions<sup>4</sup>.

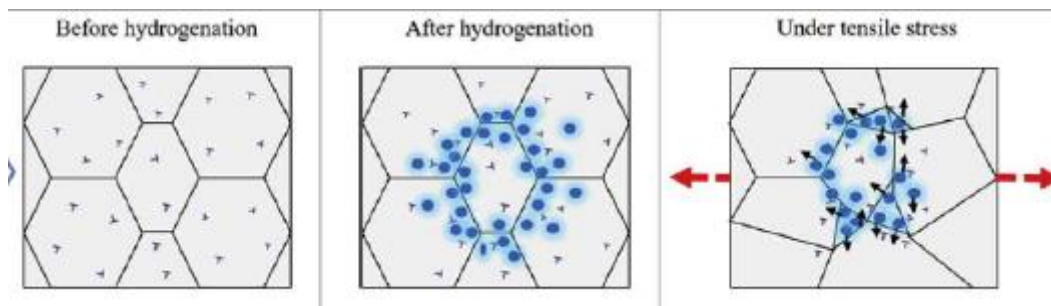


Figure 1. The mechanism of Hydrogen infiltration<sup>5</sup>.

The ultimate aim of the RecHycle project is to introduce a Hydrogen-driven steel making prototype plant. This will include a supply system, which will lead Hydrogen to the blast furnace. For the above-described reasons, it is of high importance to analyse the effect on the piping and blast furnace elements, in order to foresee any future problems in the implementation of the facility and prevent any undesired effect. For this purpose, the consortium has agreed an approach and methodology, which will be explained in the following chapter.

<sup>1</sup> Combining Machine Learning, Embedded Sensor Networks and Additive Burner Design for Combustor Structural Health Monitoring, Proceedings of the ASME Turbo Expo 2024, Turbomachinery Technical Conference and Exposition, GT2024, June 24-28, 2024, London, United Kingdom

<sup>2</sup> Stress corrosion cracking, Theory and Practice, 2011, pg 90-130

<sup>3</sup> Novel postprocessing for fatigue and hydrogen resistance of Additive Manufacturing aircraft materials, LaSPAM Project (<https://projekte.ffg.at/projekt/4121912>)

<sup>4</sup> Explosion by experiment: two researchers of TU Graz severely injured, Kleine Zeitung, [link](#)

<sup>5</sup> Huang, S., Agyenim-Boateng, E., Sheng, J., Yuan, G., Dai, F. Z., Ma, D. H., ... & Zhou, J. Z. (2019). Effects of laser peening with different laser power densities on the mechanical properties of hydrogenated TC4 titanium alloy. International Journal of Hydrogen Energy, 44(31), 17114-17126.

### 3 Definition of the work methodology

The work methodology for the evaluation of the HE was organised in the following way:

1. Analysis of the components exposed to hydrogen flow and determination of the level of impact of Hydrogen on their proper functioning during the steelmaking process. Neither all materials nor all components are equally affected by the HE. Therefore, the first step in the methodology should be a selection of the critical components of the pipeline, which supplies the Hydrogen to the blast furnace.
2. Screening of the materials used to make these components and the literature review of the impact of Hydrogen to their properties, in terms of embrittlement. The main objective of this step is to analyse the target materials, look for eventual findings already available in the literature, when it comes to their usage in a Hydrogen rich environment, and draw some initial conclusions, if these were to be prone to HE and degradation of their functionality.

These two steps will be explained in details in the following section.

3. Material testing campaign to determine this effect physically and chemically. This step consists of two main sub-steps. The first one is the definition of the properties, which can reveal the hypothetical HE, while the second one is how to perform the generation/measurement of these properties in a constrained experimental facilities – it is important to highlight that, at the beginning of the project, the prototype facility would be not be available until the 2<sup>nd</sup> half of the project. Therefore, in the proposal it was defined that the analysis of the HE would be done in the laboratory conditions. Hence, a meaningful and intelligent definition of the test procedures was important.
4. Proposition of measures to improve the component resistance to embrittlement, by proposition of protective measures (e.g., coatings) and/or other materials. Once the testing was completed, the KPIs collected, the important step is the overall evaluation of the results and conclusions in the sense of possible measures to improve the HE resistance. This would be done with an eye on the industrial feasibility of the wider deployment of the selected measure.

## 4 Definition of the material and methods

### 4.1 Components' analysis

After a dedicated analysis between AMB, AMMR and JOA, the following conclusions have been reached:

- The storage elements for Hydrogen are not of relevance in this project, rather the elements which transfer the Hydrogen stream to the furnace. The reason for this is that the main supply of the Hydrogen for the blast furnace would come from the independently located electrolyzer of big power. In that case, the Hydrogen will be transferred from the pipeline to the blast furnace using an internal pipeline, composed of the pipes and finalised by the blow lances.
- The most critical components are exposed to cold and hot temperatures. The cold end is exposed to Hydrogen at the room temperature, while the hot end has a span of temperatures that goes from the room temperature to the 1000°C, making it a much more complex scenario.

### 4.2 Materials' analysis

The next step was to perform the analysis of the materials. The Hydrogen-affected area is made of two types of materials, both HT alloys, while the cold end is made of the Sandvik Avesta. The chemical composition of the materials is shown below.

Table 1. The chemical composition of the materials

Material 1	Ni [%]	Fe [%]	Cr [%]	Rest
	57	3	22	AL, Co, Mo, W, C...

Material 2	Cr [%]	Ni [%]	Rest
	14-18	70-75	Fe...

In general, several theories have been proposed to explain the HE phenomenon; mostly, hydrogen-enhanced localized plasticity (HELP)<sup>6</sup>, hydrogen-enhanced decohesion, (HEDE)<sup>7</sup>, and adsorption-induced dislocation emission (AIDE)<sup>8</sup> mechanisms are invoked to explain the observation of failure modes in Ni alloys failed in hydrogen environment.

High temperature Nickel alloys have been widely studied. Lecoester et al have studied the fundamental mechanism of hydrogen translation through the Material 1 by an accelerated desorption of tritium from Alloy 600 at 293 K with tritiated tensile specimen, by beta-counting during straining. The tritium desorption flow from the sample is ten times larger during straining for the present experimental conditions. These results bring strong arguments in favour of *a mechanism of hydrogen transport by dislocations*. The authors also conclude that *the fracture mode may change from fully brittle intergranular at low strain rate to fully ductile at high strain rate with a mixed mode in an intermediate range of strain rate*. The change in fracture mode as a function of the strain rate depends on the microstructure, the more sensitive the microstructure the higher the strain rate corresponding to the brittle-ductile transition.

Also, the susceptibility of two precipitation-hardened nickel-based alloys, i.e., Alloy 718 and Alloy 725, to hydrogen embrittlement was studied using slow strain-rate tensile test and advanced characterization techniques<sup>9</sup>. The mechanical properties and fracture behaviour of these two alloys were compared in both hydrogen-free and hydrogen-charged conditions.

<sup>6</sup> H.K. Birnbaum and P. Sofronis: Mater. Sci. Eng. A, 1994, vol. 176, pp. 191–202.

<sup>7</sup> W.W. Gerberich, R.A. Oriani, M. Lii, X. Chen, and T. Foecke: Philos. Mag. A, 1991, vol. 63, pp. 363–76.

<sup>8</sup> S. Lynch: Corros. Rev., 2012, vol. 30, pp. 105–23.

<sup>9</sup> Lu, X., Ma, Y., & Wang, D. (2020). On the hydrogen embrittlement behavior of nickel-based alloys: alloys 718 and 725. Materials Science and Engineering: A, 792, 139785.

In the presence of hydrogen, Alloy 718 failed prevalently through a combination of transgranular and intergranular cracking behaviour, while Alloy 725 failed primarily through intergranular failure with a considerably lower resistance to hydrogen embrittlement. This distinction was attributed to their different microstructures and different types of precipitates along grain boundaries. Specifically, in Alloy 725, the decoration of (Cr, Mo)-rich precipitates at grain boundaries distort the local structures and cause such boundaries to be vulnerable to hydrogen attack, thus promoting intergranular cracking. However, it must be highlighted that *the hydrogenization was performed in ionized Hydrogen solution - in a mixture of glycerol and H3PO4 [31] for 18 h at a cathodic current density of 15 mA/cm<sup>2</sup> at 75°C.*

Obasi et al have tested the In718 and In945X. They also used a *solution hydrogenisation, more precisely Hydrogen was introduced into the material at 80°C by electrochemical charging in a sodium chloride (NaCl) aqueous solution for 7 days.* They also used slow strain rate tests (SSRTs), which were performed in air at room temperature (20°C) on both uncharged and hydrogen-charged sample. This study also offered different processing conditions of the alloys.

The conclusions taken out of the literature review are as follow:

- The few studies of the HE of Material 1 have concentrated on the fundamental investigation of the Hydrogen migration in the material, not on the industrially relevant HE study; on the other side, most of the Material 2 studies refer to the ageing and corrosion resistance;
- The industrially-oriented studies on other alloys, such as In625 and 718, are quite thorough and complete, and have focussed on Slow Strain Rate testing (also known as Constant Strain Rate testing) – this has been already found and performed by the partner JOA in other related studies of HE in Steels, Ti64, etc [already referenced LaSPAM project]. This approach has *undoubtable use in the clear detection of the elongation reduction due to the embrittlement*, but it also presents some problems, which will be mentioned in the following sections.
- Most of the testing was made using the *ionic solution of Hydrogen*, that is, the material samples have been submerged in an electrolytic solution and attacked by the Hydrogen ions, which have been recombined later in the material, once they diffused into the sample. Under our humble opinion, this is not a realistic representation of the industrial case, where the gas H<sub>2</sub> at room and very high temperatures attacks the material. If we were studying the storage of (liquid) Hydrogen, certain parallelisms could be drawn. But, in case of a gas transport through the piping, it is logical to reproduce the gas transport conditions.

In order to make a different approach, more close to the relevant industrial environment, but also contribute to the SoA with a novel approach, JOA, in agreement with the industrial partners, has chosen a different approach which will be exposed in the next section in details.

### 4.3 Definition of the testing methodology

For the material testing the following constraints have been established:

- The material should be exposed to gas in order to replicate the relevant industrial conditions;
- The exposure must be performed on both room and high temperature conditions;
- The evaluation of the effect of HE on the material properties, has to do with the fragilization of the material – due to some of the above explained mechanisms. The evaluation of the elongation before and after the Hydrogen charging is one (and predominant) approach. However, in the already mentioned national project LaSPAM (<https://projekte.ffg.at/projekt/4121912>), JOA has experimented the following problems with the CSR testing:
  - The samples for CSR, to be representative, must have a representative length (in this case, it was 120mm). This is not problematic, when the samples are exposed to an electrolytic solution, but makes it *quite challenging for the exposure in the lab setup for hydrogen flow – the sample holder and the system itself (including the amount of the Hydrogen gas in circulation) should be much bigger.* Apart from the costs, the acceptance of this kind of setup by the local authorities in Austria (but elsewhere as well) is problematic. The logistics, but also the certification of this kind of setup is exponentially growing in complexity with the size of the samples.
  - The CSR test is *not a fast test*, commonly it takes days to weeks and, with the recent increase in relevance of Hydrogen studies, the available testing facilities are relatively

busy. That would jeopardize the delivery of the results. Therefore, a need for a faster test was obvious.

- What is necessary in RecHycle, but in general for the HE evaluation, is a qualitative study and not quantitative study; we need to evaluate the effect of the Hydrogen Embrittlement on materials comparing the exposed and non-exposed material – the faster, the better.
- The metallurgical findings are of relevance, since in the literature there are several reports, which indicate the possible influence of the HE on the microstructural properties. Therefore, the metallurgical images should accompany the mechanical testing results.

Out of the above mentioned postulates, a conclusion arose that the material testing should be organized in four parts:

- **Exposure of the material to Hydrogen at room temperature** – to simulate in lab conditions the exposure of the pipes to 100% Hydrogen at the cold end<sup>10</sup>;
- **Exposure of the material to Hydrogen at elevated temperature** – to simulate in lab conditions the exposure of the lances to 100% Hydrogen at the hot end.
- **Mechanical testing of the exposed vs. non-exposed material** – to evaluate comparatively the effect of embrittlement, if any.
- **Metallurgical observations** – to spot the reasons of embrittlement, if appears, in terms of what metallurgical transformation of the material takes place to create the embrittlement.

#### 4.3.1 Exposure at room temperature

For the **exposing of the material to Hydrogen at room temperature**, a special laboratory setup was designed and implemented at JOA. The following pictures shows this setup. It was designed by JOA and implemented with the help of a specialized company from Graz, CBOne e.U., whose integrants have much more experience in the practical setups to work with the Hydrogen lab testing equipment.

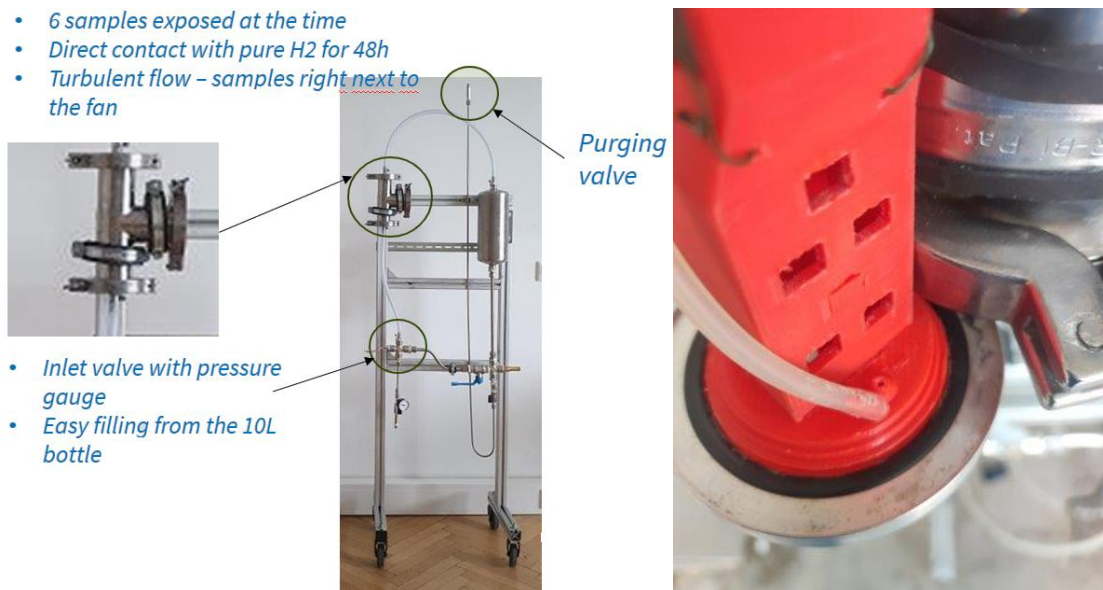


Figure 2. Hydrogenisation (H<sub>2</sub>-O) setup (left) and the sample holder (right).

The setup consists of a Hydrogen deposit (vol: 2L), which is directly connected to a 10L bottle of Hydrogen, with an one-direction valve, to ensure the easy filling of the circuit, but prevent the loss of the gas. The filling for each testing is done until the pressure in the deposit is between 4.5 and 5 bar. The circuit ensures the flow of the Hydrogen by a slight over pressure (150 mbar) in the sample holder and a fan which is installed right at the entrance of the sample holder. The sample holder lodges 6

<sup>10</sup> The hot end materials are subdued to the transition between cold and hot temperatures, as they are crossing through the tuyeres. So it is meaningful to test them at cold and hot temperatures.

transversally positioned samples, which are exposed to a laminar or turbulent regime, according to the settings of the fan (in our case, it was set to turbulent, to promote more Hydrogen contact with the sample). The system was tested to withstand more than 60h, until the pressure reaches 1.5 bar (the pressure below this value would create conditions for the entrance of air and possible deflagration). After 48h of testing, it normally reaches 1.7-1.8 bar, sometimes even remains at 2.0 bar (depending on the atmospheric pressure of the surrounding). Hence, the end of **the test was set as 48h after the start** upon this test results, but also for three more reasons:

1. The literature has shown exposure times of down to 7h to up to 7 days. Therefore, the selected exposure time fits into this timespan;
2. The period of 48h has shown in previous projects to be more than enough to clearly denote the HE effect, e.g. in the case of electrolysis cell of Titanium samples;
3. The exposure times at room and high temperature should be the same, so the selection of the time was also conditioned by the HT exposure facilities (BORIS furnace, see a bit later).

After each test, the system is purged using a purging valve, to eliminate all traces of Hydrogen for safety reasons. Then the samples are evacuated.

Hence, the tests were performed at the regime of 48h, 6 samples at the time. During the testing, an electronic-powered network of sensors is constantly measuring the main parameters (speed, temperature, pressure, etc.). These are then exported as a .csv file to the computer from the microcontroller board.

#### 4.3.2 Exposure at the high temperatures

The **exposure of the material to elevated temperatures** has taken place at 1000 °C, and was carried out at AMMR, in the BORIS furnace. The following Figure shows details of this equipment. The main features that made this equipment selected for the HT exposure are:

- it can be flooded with many different gases, among which is a 100% H<sub>2</sub>;
- it can reproduce a broad range of thermal profiles, up to high temperatures and
- a large amount of test samples of small size can be simultaneously exposed in it.

The idea was to replicate the 48h cycle, just like at room temperature. However, due to safety reasons, the cycle has been achieved using 5 exposure during the daytime shift, when the furnace could be observed and controlled. That, on practical level, meant {5 exposures = 4 days x 10h + 1 day x 8h} using pure H<sub>2</sub> at 1000°C - the cycles would be dependent on the possibilities of AMMR. Between the individual exposures, overnight, the samples have been flooded with inert gas – N<sub>2</sub> to keep them away from the oxygen influence.

After charging, the samples have been sent to JOA for metallurgical/mechanical properties testing.

#### 4.3.3 Mechanical testing of exposed and non-exposed samples

In the introduction of the Section 4, it was explained why the CSR or SSRT tests were not selected. Actually, in the proposal stage this was proposed, but the findings explained above were discovered in the projects, which findings came later.

The selected method is **fatigue testing using a Mini FP machine** (see the figure below). We could say that the fatigue behaviour decrease has been widely related to the HE<sup>11,12</sup>. It is true that the fatigue and CSR testing share one problem – *the testing is time consuming*. Therefore, normally, we would also avoid fatigue testing as a comparative, qualitative method of HE evaluation. However, the Mini FP has established a breakthrough in this sense.

---

<sup>11</sup> Lokhande, K., & Vishwakarma, M. (2022, July). In IOP Conference Series: Materials Science and Engineering (Vol. 1248, No. 1, p. 012026). IOP Publishing.

<sup>12</sup> Adasooriya, Nirosha D. ISOPE International Ocean and Polar Engineering Conference. ISOPE, 2023.



Figure 3. Mini FP2 testing equipment.

This compact equipment is normally used to evaluate dynamic properties of small samples, which have been manufactured using different process conditions (casting, welding, 3d printing). So, during the process development, it is used to qualitatively ensure which process conditions can give better dynamic performance of the obtained material. Without preclusion, it can be used for *any comparative study*: post processing, chemical exposition of samples – whenever the dynamic properties of the material are a revealing factor – in this case it is, since the embrittlement reduces the tenacity of material and reduces its dynamic performance.

The biggest advantages of this testing procedure for RecHycle are:

- According to the literature, the dynamic behaviour is *directly correlated to embrittlement*, so the lower fatigue performance can reveal higher level of HE – be it crack initiation or formation of brittle compounds inside of the microstructure;
- The samples used in the Mini FP have quite small dimensions (7x5x22mm) and are *reducing the volume of the lab setup for H2 charging significantly*: the volume of Hydrogen in circulation, the deposit, the sample holder and – the most important – the safety issues. The setup for exposing the 6 samples at a time circulates the quantity of the Hydrogen, which has the thermal energy of a cigarette lighter. This makes the testing facility much safer and easier to use, as well as the obtaining of the permission of the local authorities.
- The testing procedure in MINI FP2 is *very fast* – the entire Wöhler curve can be accomplished in 20-25 days, while the hydrogenisation of all necessary samples for one Wöhler curve (15) takes 3 batches of 5 samples x 48h = 6 days. So, the testing for any material or any material condition can be accomplished in 1 month.

The hydrogenisation and testing were done in parallel, to be able to start drawing conclusions as we were progressing.

#### 4.3.4 Metallurgical analysis

Despite of the revealing capacity of the mechanical testing, it is considered that the metallurgical analysis of the material samples cuts would be quite interesting, in case we could detect some changes in the microstructural state of the samples before and after the H<sub>2</sub> exposure. Additionally, as a double check method is also quite useful, to confirm the mechanical testing findings.

To this aim REM-TESCAN equipment, based on Scanning Electron Microscopy (SEM) at JOA has been widely used. The following figure shows the equipment. SEM is a well-known non-destructive technique that uses an electron beam probe to analyse samples surface down to nano-scale. The SEM produce high magnification images with high resolution, a feature of which makes them suitable tools for a wide range of applications in numerous fields of science and industry, such as the comparative analysis of the microstructural states. The one at JOA is also equipped with the EDX, so, to certain extent and precision, the chemical composition can be also evaluated.



Figure 4. TESCAN's SEM equipment.

## 5 Results and discussion

### 5.1 Material selection and sampling

The original idea was to use the real unused components to make the samples for testing. Therefore, AMB has sent a number of relevant ones made out of the target materials to JOA for the sample preparation (**Error! Reference source not found.**). However, a problem occurred. Once cut in samples, these were not perfectly flat – therefore, they could not be used in the Mini FP machine. They were mechanically flattened, by using a pressing machine, and several of them (non-exposed) were tested. Luckily, it was done before the Hydrogen exposure started since it was discovered that the flattening – although it seemed relatively small – introduced significant plastic deformation and related microstructural change. Therefore, samples were simply incomparable.

As a consequence, a decision was made to buy a flat material, rolled just in the case of the lances, but not rolled into a tubular shape. It was challenging but successful task, since that kind of material was found at Goodfellow in a relatively small piece (Material 1: 100x100x5.25mm, in foil; Material 2:  $\varnothing$ 25.4x100, in rod)). This was of significance, because the price of a sheet with dimensions of 1 x 2 m, and 5mm thickness, has a price of 8.000 and 12.000 €, for Material 1 and Material 2 alloy, respectively, which would be unaffordable for the project budget of JOA.

In the first place, as a contrasting measure, the received materials were contrasted with the one from the AM real components.

#### **Material 1**

The analysis showed that the Material 1 Alloy received from Good Fellow and the one of the AM components have shown the same phase – namely the  $\gamma$  matrix phase.

- Arcelor Mittal blow lance: grain size: 20 – 80  $\mu\text{m}$ ,  $\gamma$ -matrix; No  $\gamma'$  or  $\gamma''$  phase or  $\delta$  phase and small amount of inclusions
- Good Fellow foil: grain size: 100- 200  $\mu\text{m}$ ,  $\gamma$ -matrix; No  $\gamma'$  or  $\gamma''$  phase or  $\delta$  phase and small amount of inclusions

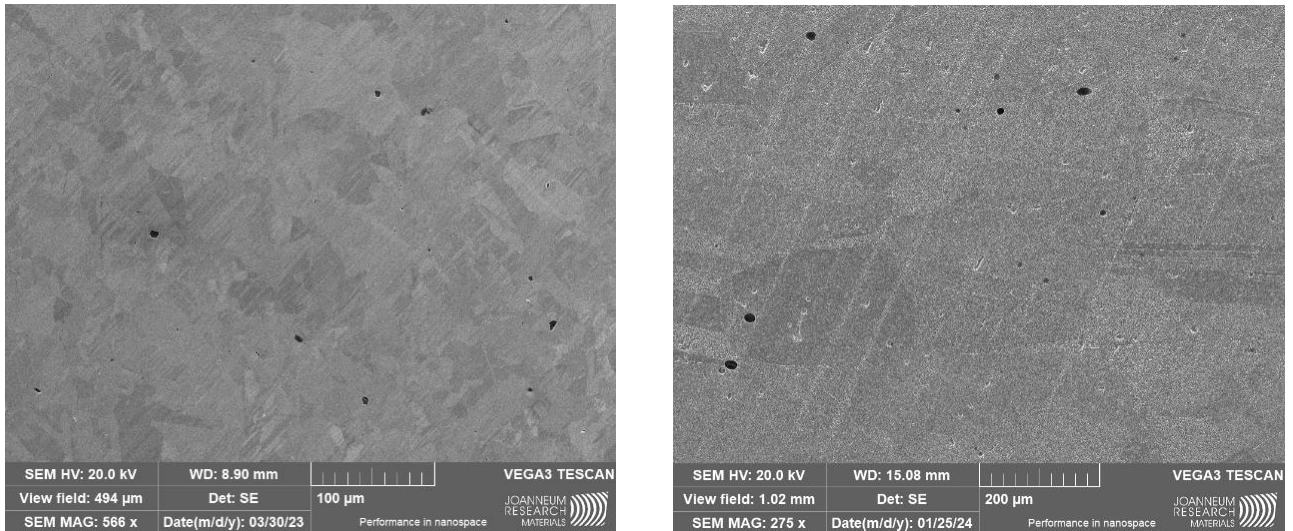


Figure 5: The microstructure overview of the as-received Material 1 pipe of Arcelor Mittal (left) and the Material 1 plate from Good Fellow (right)

However, it was detected that the Goodfellow material has a relevant number of pores.

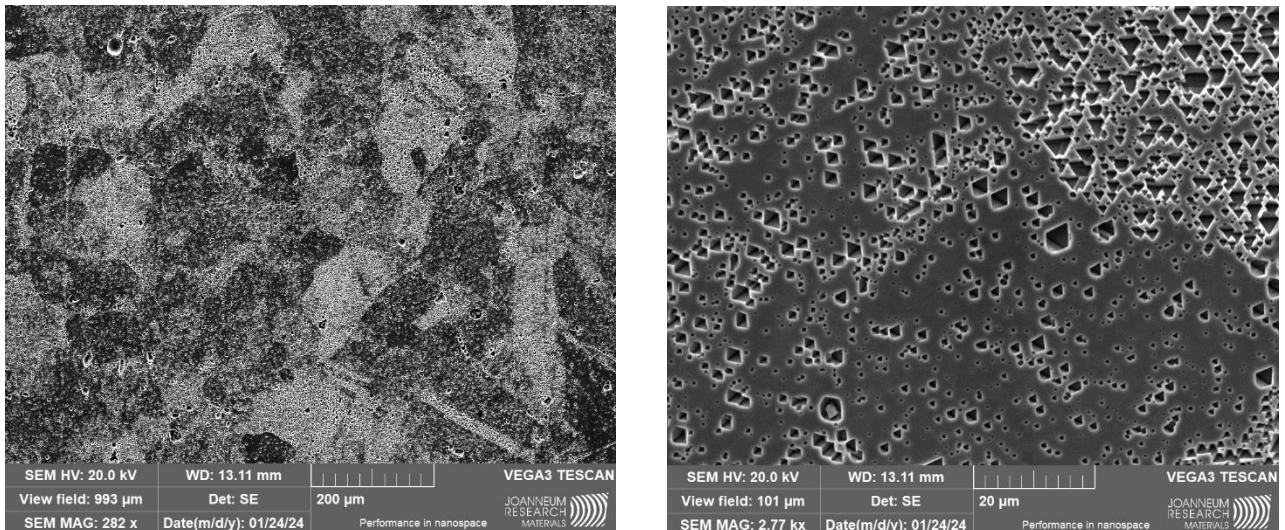
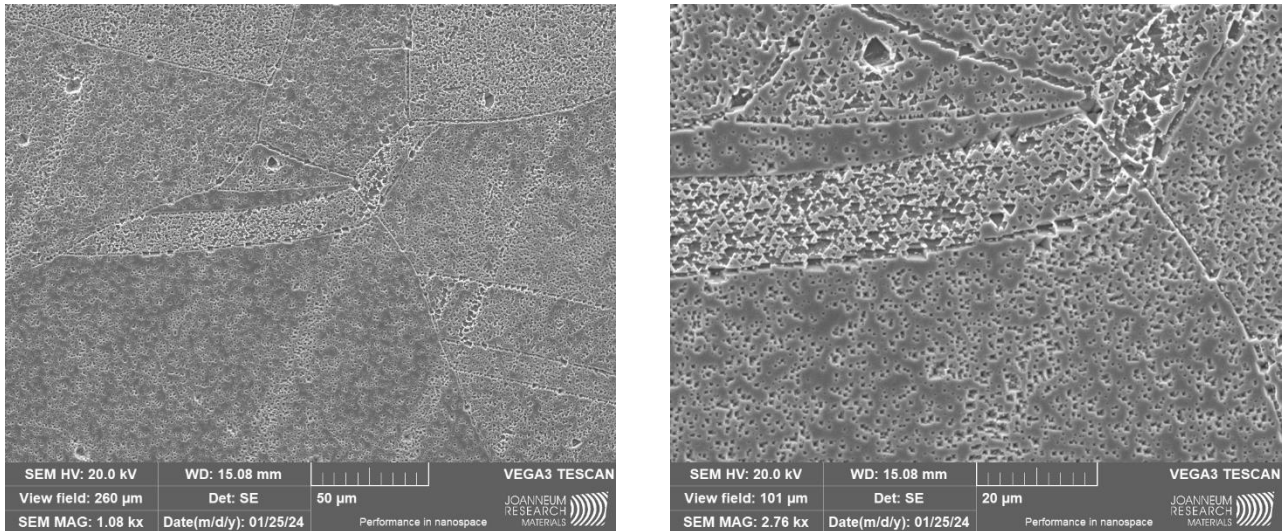


Figure 6: The microstructure of the as-received Material 1 plate depicting the pores and cavities at the surface

The cavities and pores were analysed with EDX and revealed the same chemical composition as the rest of the material, indicating that the pores were formed during the manufacturing process. The cross sectional area of the material was analysed next, to see if the cavities and pores are only surface prone, or if they also are found within the bulk of the material.



*Figure 7: The microstructure of the as-received Material 1 plate depicting the pores and cavities from the cross section of the material*

The cavities and pores are present throughout the whole bulk of the material (Figure 7 left and right). Nonetheless, the material was still used for hydrogen charging even though pores and cavities are present mainly for two reasons:

1. The material was to be used for a comparative study – being this porosity a constant factor in uncharged, RT charged and HT charged Material 1. Unless it would give a drastically low results, incomparable among themselves, it should not present a problem;
2. Also, buying an alternative material on the market was quite difficult.

### **Material 2**

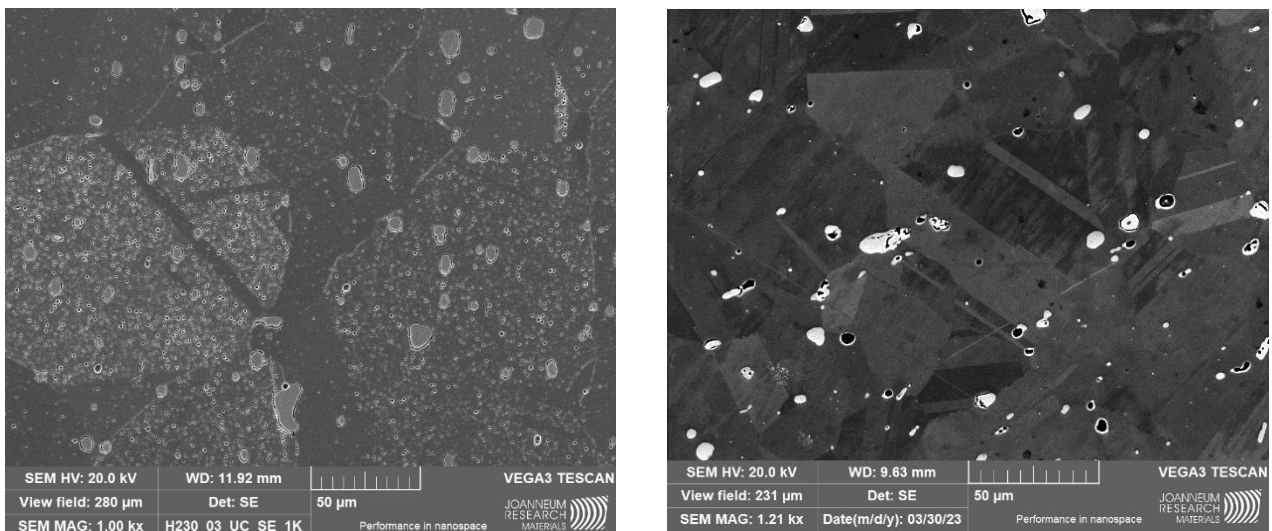


*Figure 8: Haynes Alloy from Good Fellow Rod (left) vs. the Material 2 pipe from Arcelor Mittal (right)*

The Goodfellow rod shows more tungsten particles within certain grains, but overall the tungsten percentage is the same as within the material of Arcelor Mittal, which was proven by EDX analysis. The grains of the Goodfellow rod show bigger grains which lie above  $>100\ \mu\text{m}$ , whereas the grains of Arcelor Mittal are smaller. The tungsten particles within the Arcelor Mittal specimen are more scattered throughout the material and are not centred along the grains and within the grains. Even though the highly centred tungsten particles could cause HE when charged this is not the case as shown in this further study, therefore we can conclude that the material of Arcelor Mittal should also withstand the conditions of hydrogen charging for 48h.

## 5.2 Material charging procedure

### 5.2.1 Procedure at room temperature

The metal samples were mounted into the sample holder shown in Figure 2 right. Pure hydrogen with turbulent flow conditions of approx. 10 m/s circulates through the device with a pressure starting at >4 bar. The samples are mounted directly behind the ventilation system in order to establish a turbulent flow regime. The sensor system purchased with the device did not correctly show the pressure and had an error of  $\pm 60\%$  of the value obtained manually from the pressure gauge. Unfortunately, there was no time within the project to return the device for a proper sensor reset and the device was used as it was and the values were obtained manually from the pressure gauge.

Material 1 Alloy RT Testing was performed in the following batches:

#### Batch 1: (16.10-18.10.2023)

Differential pressure [Pa]	Temperature [°C]	Pressure [bar]
390	3 – 12	2.3 - 4.1

#### Batch 2: (23.10-25.10.2023)

Differential pressure [Pa]	Temperature [°C]	Pressure [bar]
34-390	12 - 16	2.8 - 4.2

The differential pressure for the Batch 2 went down due to an mishandling of the sample holder, which led to the broken pin. Nonetheless, the resulting differential pressure drop (35Pa) has not affected the hydrogen testing for this batch of samples and therefore the sample was further charged for another 24 hours with a differential pressure below 100 Pa. The sample holder was then printed again and after changing it, the pressure did not drop below 300 Pa for further tests.

#### Batch 3: (31.10-02.11.2023)

Differential pressure [Pa]	Temperature [°C]	Pressure [bar]
310-410	7 – 16	1.8 - 4.2

For all three tests the temperature varies depending on the daily situation as the test set up was built up outside because of safety reasons. Nevertheless, we have a temperature range from 0 – 16 °C which will be sufficient to compare to non-hydrogenated samples and the samples hydrogenated at 1000 °C.

Material 2 RT Testing was also done in batches:

#### Batch 1: (06.11-08.11.2023)

Differential pressure [Pa]	Temperature [°C]	Pressure [bar]
310 - 350	6 – 11	1.8 - 4.4

#### Batch 2: (08.11-10.11.2023)

Differential pressure [Pa]	Temperature [°C]	Pressure [bar]
340-395	7 - 10	1.7 - 4.7

#### Batch 3: (14.11-16.11)

Differential pressure [Pa]	Temperature [°C]	Pressure [bar]
310-370	7 – 9	1.6 - 4.2

## 5.2.2 Procedure at high temperature

17 samples of Material 1 and 17 samples of Material 2 were sent to AMM by JOA to be hydrogen charged at high temperature. The procedure defined by the AMM was:

- Samples are placed between two beds of alumina beads
- Usable volume will be a tube of 80\*4 cm
- Gas flow: 900 NI/hours
- Max. t°C: 1000 °C
- Gas composition: H2 at 100 %
- Tests will be carried out by 8-10 hours sessions, with chemical quenches during the night using N2

Tests were carried out starting on 10.01.2024 over the time frame of 6 days. Technical parameters are given in the table below:

Temperature [°C]	H2 flow [l/h]	Size of tube [cm]
1000	900	4

After the charging, the samples were packed and returned to JOA for mechanical testing.

## 5.3 Fatigue testing of the samples

### 5.3.1 Material 1 dynamic properties

The following figure shows the comparison of *the Wöhler curves of Material 1 samples uncharged, charged at RT and charged at HT*. The potential curves have been calculated using the raw data values and extrapolating a potential model which fits best to the data obtained by the measurement. *Three different f(x) values were obtained through the power law fit (f(x) = y0 + A \* x<sup>pow</sup>), for all three conditions (the uncharged, RT charged and HT charged) and then used to calculate a mean corrected value for 500 MPa, 450 MPa and 400 MPa loads.*

$$\text{Material 1 uncharged: } f(x) = -30.192 + 2348.11 * x^{0.11212}$$

$$\text{Material 1 RT charged: } f(x) = 377.22 + 2.7 * 10^{10} * x^{-1.3803}$$

$$\text{Material 1 HT charged: } f(x) = 3378,1x^{-0.142}$$

The values were then used for the calculation of HE [%], as shown in the equation below:

$$HE [\%] = \frac{\text{Cycles Charged}}{\text{Cycles of Uncharged}}$$

The ratio of the cycles charged to cycles uncharged at a certain stress value determines the hydrogen embrittlement. The values obtained can be found in the table below. It is important to state that the hydrogen infiltration did not decrease the cycles and therefore, the dynamic properties, it even turned out to increase the cycles. Another important factor which was taken into consideration is the statistical error of the fatigue machine. The raw data at a certain maximum stress value tend to show a certain standard deviation, which we included in the calculation to obtain correct results.

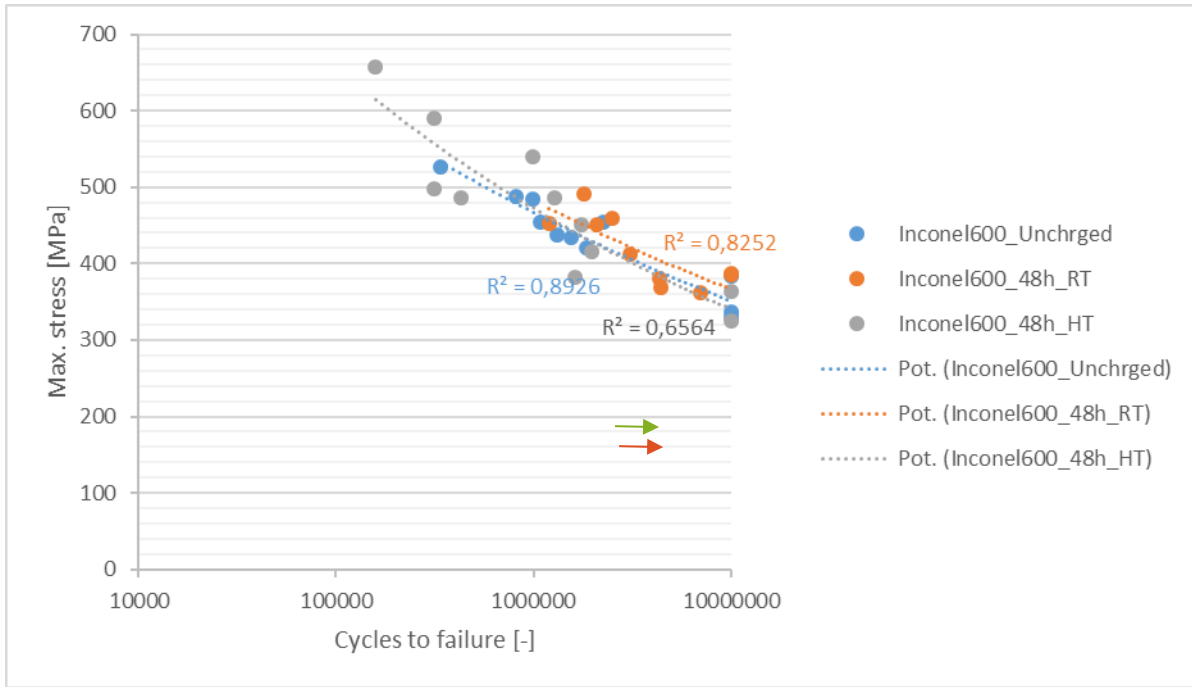


Figure 9: Wöhlercurve of Material 1 Alloy uncharged vs. Material 1 Alloy 48h charged at RT vs charged at HT

The values selection followed the literature. Lima et al<sup>13</sup> did the testing of Inconel 625 with the range of loads 350 and 550MPa, starting at the mid-value of 450MPa, so for Material 1 we followed the same range.

The table below represents the findings explained above. As stated above, the comparison was made tracing the values on the potential curves corresponding to the selected loads, but then the obtained values were corrected using the *standard deviation of the fatigue machine* (calculated using real values at the similar load<sup>14</sup>), to *extrapolate the mean deviation*. Therefore, although the potential curves visually induce to think that the material even got stronger with the hydrogen exposure, actually the HE factor is below 1%, including the statistical error of the machine, for the RT and HT charged material.

Table 2: Calculated number of cycles at pre-defined max. stress according to the power fit of the uncharged Material 1 Alloy

Max. Stress [MPa]	N90% [cycles]	HE [%]
500	581047	/
450	1405698	/
400	3747988	/

Table 3: Calculated number of cycles at pre-defined max. stress according to the power fit of the RT charged Material 1 Alloy; The resulting HE factor with and without the correction through the statistical error of the machine

Max. Stress [MPa]	N90% [cycles]	HE [%]	HE [%] with standard deviation of fatigue machine

<sup>13</sup> Lima et al. Materials Research. 2018; 21(4): e20171089

<sup>14</sup> The real value of the machine load was read from the machine directly.

500	1.110.139	+91%	+0,019%
450	1.625.613	+15%	+0,0015%
400	3.823.646	+2%	+0,0011%

*Table 4: Calculated number of cycles at pre-defined max. stress according to the power fit of the HT charged Material 1 Alloy; The resulting HE factor with and without the correction through the statistical error of the machine*

Max. Stress [MPa]	N90% [cycles]	HE [%]	HE [%] with standard deviation of fatigue machine
500	693.594	+19%	+0,0012%
450	1.456.258	+4%	+0,001%
400	3.336.968	-11%	-0,0011%

It can be concluded that the dynamic mechanical properties do not change after hydrogenation for 48h. The hydrogen charging did not affect the material and no failure of the material can be observed. This will be further confirmed with metallurgical and fracture analysis in the next section.

For further info, the following tables show the raw data of the testing. The N(x) just indicates at which percentage of the threshold the measurements are stopped when the material is broken or crack nucleation has occurred. So, for N 40% corresponds to a drop of the force to 40 % of its initial value and N 90% corresponds to a drop of force to 90% of its initial value.

*Table 5. Sample dimensions, number of cycles at 40% and 90% respectively and the maximum stress applied - uncharged.*

c [mm]	s [mm]	h [mm]	l [mm]	N <sub>40%</sub> [cycles]	N <sub>90%</sub> [cycles]	$\sigma$ max. [MPa]
5.26	4.84	6.94	21.63	1860000	1557000	434.14
5.27	4.98	6.81	21.59	375000	337000	526.01
5.30	4.94	6.97	21.61	1162000	1086000	453.60
5.28	4.99	6.97	21.57	10000000	10000000	329.88
5.28	4.91	6.83	21.50	1480000	1316000	437.37
5.27	4.95	6.88	21.43	1101000	997000	484.19
5.27	4.99	6.97	21.57	2646000	2247000	454.67
5.27	4.97	6.98	21.48	2047000	1867000	420.28
5.28	4.87	6.82	21.51	909000	821000	487.26
5.27	4.80	6.72	21.67	10000000	10000000	384.48
5.27	4.78	6.84	21.66	10000000	10000000	337.08

*Table 6. Sample dimensions, number of cycles at N<sub>40%</sub> and N<sub>90%</sub> respectively and the maximum stress applied – charged at RT for 48h.*

c [mm]	s [mm]	h [mm]	l [mm]	N <sub>40%</sub> [cycles]	N <sub>90%</sub> [cycles]	σ max. [MPa]
5.26	4.96	6.93	21.69	2211000	2085000	451.17
5.28	4.95	6.94	20.59	2730000	2495000	460.09
5.27	4.88	6.94	21.17	3463000	3106000	411.68
5.30	4.95	6.91	21.52	4804000	4399000	367.85
5.31	4.91	6.91	21.56	5055000	4336000	380.93
5.33	5.00	6.88	21.44	1369000	1200000	452.95
5.34	5.02	6.90	21.43	7721000	6969000	361.74
5.36	5.02	6.88	21.54	10000000	10000000	387.07
5.38	4.96	6.95	21.40	10000000	10000000	386.27
5.38	5.01	6.91	21.44	1961000	1802000	491.24

Table 7: Sample dimensions, number of cycles at N<sub>40%</sub> and N<sub>90%</sub> respectively and the maximum stress applied – charged at HT for 48h

c [mm]	s [mm]	h [mm]	l [mm]	N <sub>40%</sub> [cycles]	N <sub>90%</sub> [cycles]	σ <sub>max</sub> [MPa]
5,22	5,24	6,2	22,06	1870000	1746000	450,84
5,27	5,01	6,91	21,08	206000	159000	657,07
5,28	4,94	6,89	20,68	478000	312000	589,94
5,3	5,01	6,91	21,44	1362000	1276000	486,24
5,29	4,96	6,92	20,66	2190000	1976000	416,11
5,27	4,99	6,91	21,75	522000	432000	486,77
5,29	4,83	6,51	20,63	1927000	1617000	382,41
5,24	4,99	7,03	20,92	1043000	987000	540,24
5,24	4,83	6,54	20,52	360000	314000	498,71
5,38	5,01	7,03	21,18	10000000	10000000	363,18
5,38	5,06	7,04	20,92	10000000	10000000	325,14

### 5.3.2 Material 2 dynamic properties

In similar manner as described above were obtained the three Wöhler curves are depicted below. One of uncharged samples, one of the RT charged samples and one of the samples charged at 1000°C. Basically, the same strategy was used as for the Material 1 Alloy, except different maximum stress values were chosen due to the difference in mechanical properties of the material. The following max. stress values of 700 MPa, 600 MPa and 500 MPa were used. The following power law fits were obtained for different conditions:

$$\text{Material 2 uncharged: } f(x) = 301.86 + 34851 * x^{0.38531}$$

$$\text{Material 2 RT charged: } f(x) = 377.22 + 70049 * x^{0.44817}$$

$$\text{Material 2 HT charged: } f(x) = -1145 + 3373 * x^{0.050964}$$

The Wöhler curve comparison for Material 2 is shown next, followed by the calculation of the HE index, in the same manner like with Material 1.

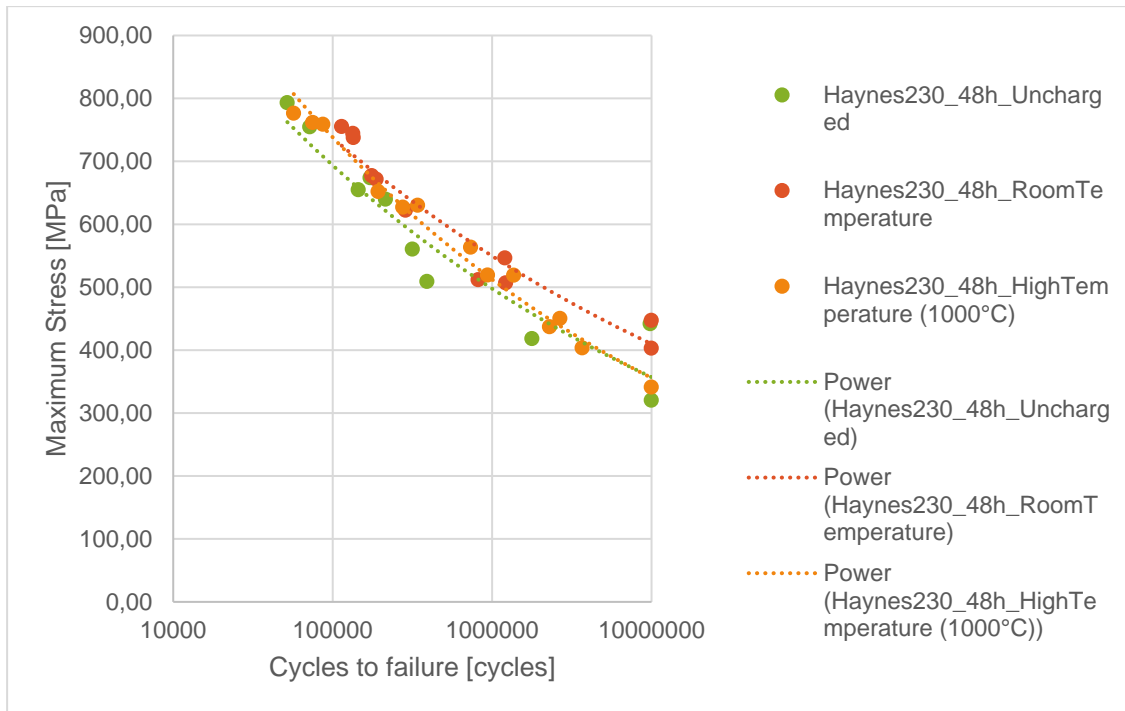


Figure 10. Wöhler curve of uncharged, RT charged and HT charged Material 2 alloy specimens, with the potential curves extrapolated upon the raw data.

Table 8: Calculated number of cycles at pre-defined max. stress according to the power fit of the uncharged Material 2 Alloy

N90% [cycles]	Max. Stress [MPa]	HE [%]
700	109692	/
600	232581	/
500	507485	/

Table 9: Calculated number of cycles at pre-defined max. stress according to the power fit of the RT charged Material 2 Alloy; The resulting HE factor with and without the correction through the statistical error of the machine

Max. Stress [MPa]	N90% [cycles]	HE [%]	HE [%] with standard deviation of fatigue machine
700	163460	+49 %	+0.15%
600	373869	+61%	+0.16%
500	1412746	+178%	+0.0027%

*Table 10: Calculated number of cycles at pre-defined max. stress according to the power fit of the HT charged Material 2 Alloy; The resulting HE factor with and without the correction through the statistical error of the machine*

Max. Stress [MPa]	N90% [cycles]	HE [%]	HE [%] with standard deviation of fatigue machine
700	138494	+26%	+0.13%
600	413174	+78%	+0.018%
500	1315327	+159%	+0.0026%

The corrected by the statistical deviation hydrogen embrittlement factor for Material 2 also lies below 1% and shows that the material withstands hydrogen atmosphere at room temperature but also at 1000 °C for 48h. We can also see an increase in cycles at the same maximum stress levels for both RT and HT charged samples. So the hydrogen atmosphere could hypothetically be increasing the dynamic properties of the material rather than decreases them within the first 48h of exposure. However, this increase, just like in the case of Material 1, can be considered statistically insignificant.

The dimensions of the specimens as well as the cycles to failure and ultimate stresses are shown in the tables below.

*Table 11. Sample dimensions, number of cycles at N<sub>40%</sub> and N<sub>90%</sub> respectively and the maximum stress applied – uncharged.*

c [mm]	s [mm]	h [mm]	l [mm]	N <sub>40%</sub> [cycles]	N <sub>90%</sub> [cycles]	σ max. [MPa]
<b>4.94</b>	5.10	6.79	21.97	10000000	9835000	441.80
<b>4.88</b>	5.11	7.03	21.87	92000	72000	754.57
<b>4.99</b>	5.11	7.01	21.92	207000	172000	673.87
<b>4.92</b>	5.18	7.03	22.03	179000	145000	654.80
<b>4.98</b>	5.01	6.92	21.91	390000	317000	560.36
<b>4.97</b>	4.99	6.89	21.91	433000	391000	508.98
<b>4.94</b>	5.03	6.97	21.85	242000	215000	639.80
<b>4.84</b>	5.11	6.88	21.92	1983000	1779000	418.07
<b>4.92</b>	5.02	6.99	21.91	10000000	10000000	320.13

*Table 12. Sample dimensions, number of cycles at N<sub>40%</sub> and N<sub>90%</sub> respectively and the maximum stress applied – charged at RT for 48h.*

c [mm]	s [mm]	h [mm]	l [mm]	N <sub>40%</sub> [cycles]	N <sub>90%</sub> [cycles]	σ max. [MPa]
4.90	4.98	6.99	21.87	156000	135000	737.64
4.99	4.99	6.92	21.85	139000	114000	755.16
4.95	5.09	7.01	21.82	165000	134000	744.26
4.87	5.14	7.05	22.02	201000	176000	676.96
4.98	5.12	7.00	22.01	217000	188000	671.39
4.97	5.05	6.96	21.97	331000	287000	622.10
4.94	5.03	7.02	22.02	904000	820000	511.80
4.87	4.93	6.98	21.84	1297000	1220000	506.75
4.87	4.91	6.84	21.86	1390000	1206000	546.28
4.80	4.94	6.93	21.84	10000000	10000000	402.86
4.84	4.94	6.83	21.88	10000000	10000000	447.16

Table 13. Sample dimensions, number of cycles at N<sub>40%</sub> and N<sub>90%</sub> respectively and the maximum stress applied – charged at HT for 48h.

c [mm]	s [mm]	h [mm]	l [mm]	N 40% [cycles]	N 90% [cycles]	σ max. [MPa]
4.91	5.06	6.73	21.89	64000	57000	776.37
5.01	5.13	6.99	21.95	93000	87000	758.59
4.95	5.09	7.07	21.87	85000	75000	761.55
4.97	5.05	6.98	21.83	205000	193000	651.80
4.96	5.07	6.96	21.99	301000	276000	627.00
4.98	5.10	6.95	21.89	356000	342000	630.02
4.96	5.04	6.92	22.01	999000	734000	563.46
4.95	5.05	6.96	22.00	999000	938000	519.10
4.89	5.03	6.95	22.05	1390000	1368000	518.86
4.95	5.10	6.83	21.98	3859000	3681000	403.30
4.95	5.03	6.94	21.92	2792000	2668000	450.24
4.91	4.96	6.77	21.97	2436000	2298000	437.09
4.98	4.88	6.71	21.91	10000000	10000000	341.00

## 5.4 Metallurgical investigations

### 5.4.1 Microstructural analysis of the fatigue samples

#### Material 1

Here, samples were taken of uncharged, charged at RT and charged at HT condition material and their chemical composition and microstructure have been compared.

Before we discuss the results, we should clarify that the chemical composition is fruit of the EDX (Energy Dispersive X-ray spectroscopy) measurement, directly on the SEM, as the below shown microstructural images were made. This method is not so precise and the fluctuation in the results are common, as well as failing to detect organic elements and gases. However, the related database accounts with this imprecision, when detecting which material is in question.

The findings were the following:

Table 14: Atomic weight percentage of the uncharged, RT and HT Material 1 Alloy; Sample 3.2

	Ni [%]	Cr [%]	Fe [%]	C [%]	Al [%]	Si [%]	Mn [%]
Uncharged	57.8	15.6	7.8	15.6	0.7	0.3	0.3
RT 48h	57.0	18.4	7.7	14.9	n/c	0.5	0.3

1000 °C 48h	63.63	16.2	8.4	11.2	0.6	n/c	n/c
----------------	-------	------	-----	------	-----	-----	-----

\* n/c - non conclusive measurement,

The atomic weight percentage of the material does not change drastically after the hydrogenation process which can be seen in the table below, indicating no hydride formation within the material. The carbon content also stays the same range and therefore also no additional carbide formation can be found due to the process.

The *RT charged specimen* were first observed under the SEM after being used in fatigue testing. The following cracks, which can be seen within Figure 11, are the result of the fatigue measurements. However, the underlying microstructure did not change significantly after the charging, in comparison to the original Material 1 microstructure. The BSE images indicate an equiaxed microstructure and the specimen have a relatively uncomplicated microstructural phase namely the  $\gamma$  phase with Cr-rich Carbides and the absence of the  $\gamma'$  forming elements [Ref]. The grain size  $>50 \mu\text{m}$ . The grain size is also important for the hydrogen embrittlement, as smaller grain sizes have a higher propensity for cracking as stated by Fabien Leonard<sup>15</sup>. The grains are quite nicely visible and the grain boundaries can be seen at magnifications of  $20 \mu\text{m}$ . The carbides do not play a significant role as there are not many scattered within the material. Therefore, the absence of the intergranular and intragranular carbides could be a reason why the material is not affected by the hydrogen infiltration.

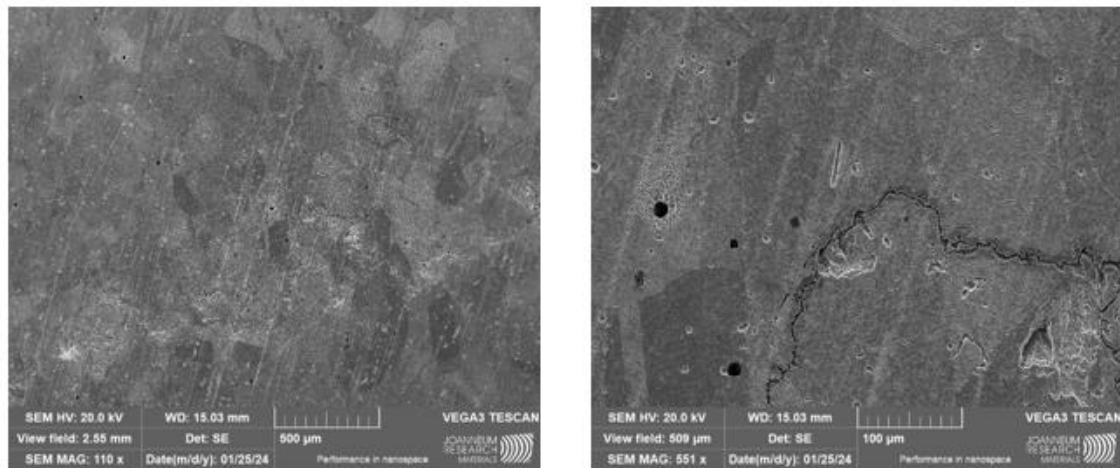


Figure 11: The microstructure of the 48 h RT hydrogen charged Material 1 plate depicting the pores and cavities from the cross section of the material. Left: Microstructure does not change, No evident hydrides or other formations between the grains. Right: Crack that formed through fatigue testing.

The different cross sectional areas of a different RT charged specimen were analysed to ensure no crack formed in the presence of hydrogen. The following figures are from different specimens/sections, where no cracks were observed and the comparison of hydrogen – charged to uncharged specimen show no signs of hydrogen embrittlement. However, the pores from the manufacturing process have been continuously observed.

<sup>15</sup> Fabien Leonard, Study of Stress Corrosion Cracking of Alloy 600 in High Temperature High Pressure water, PhD Thesis, University of Manchester, 2010.

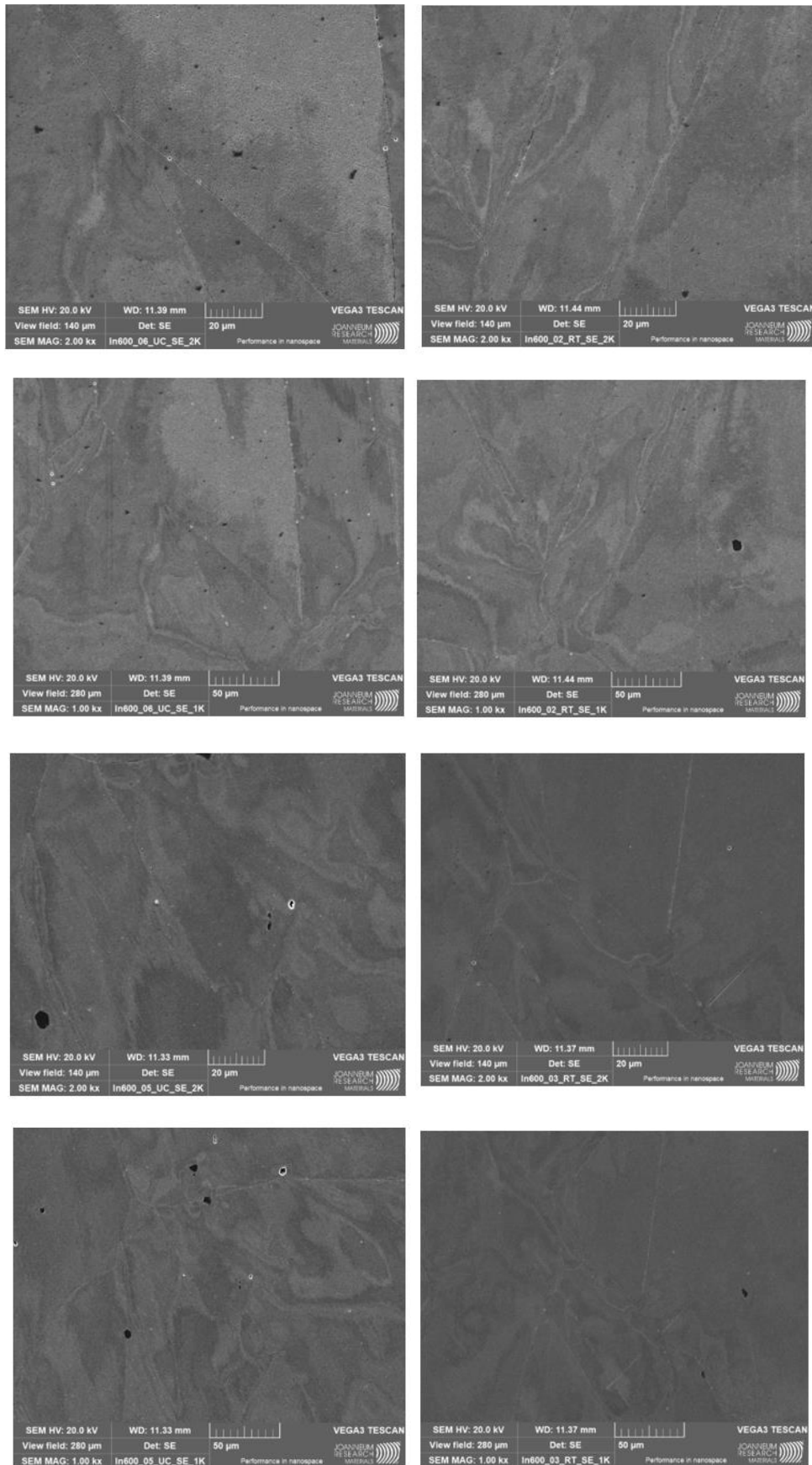


Figure 12: SEM images of different sections/samples to show the absence of the Hydrogen induced cracks and microstructural changes in RT charged samples

High Temperature (1000°C) hydrogen charged specimen are shown below. They were also investigated and the results are presented in the images below. The grains do not change in size due to the high temperature which was applied during the process, furthermore the carbides within the material do not deteriorate within the material and no cracks or pores can be found near the grain boundaries, nor at the carbides scattered throughout the material. If hydrogen embrittlement occurs, it would most likely occur at the carbide inclusions as these are defects within the material. This however does is not the case for this material.

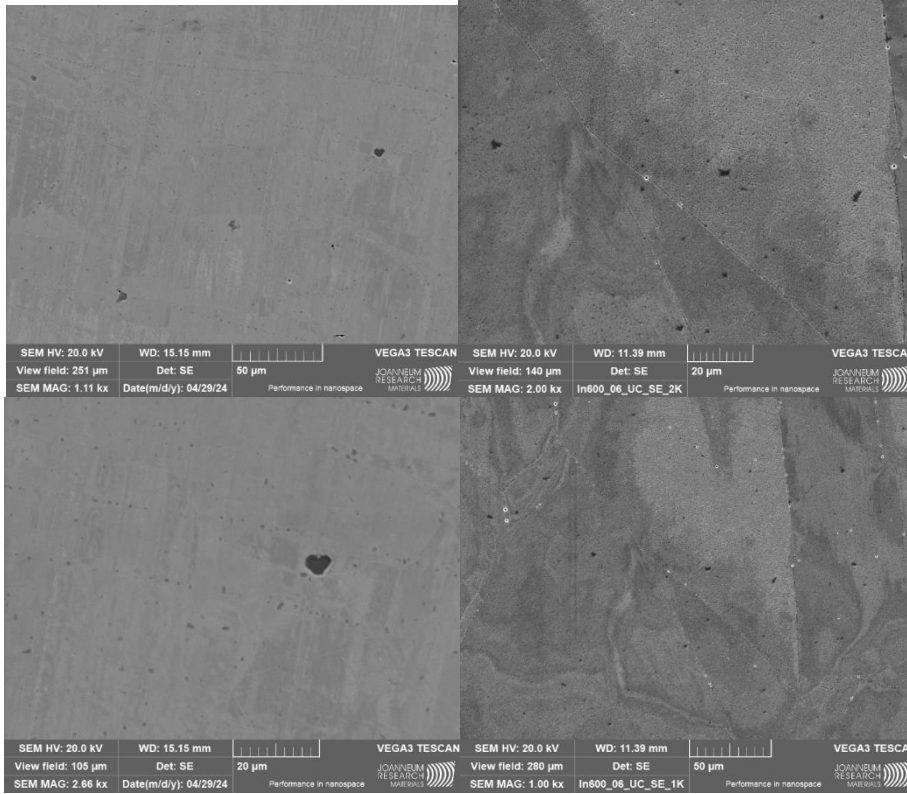
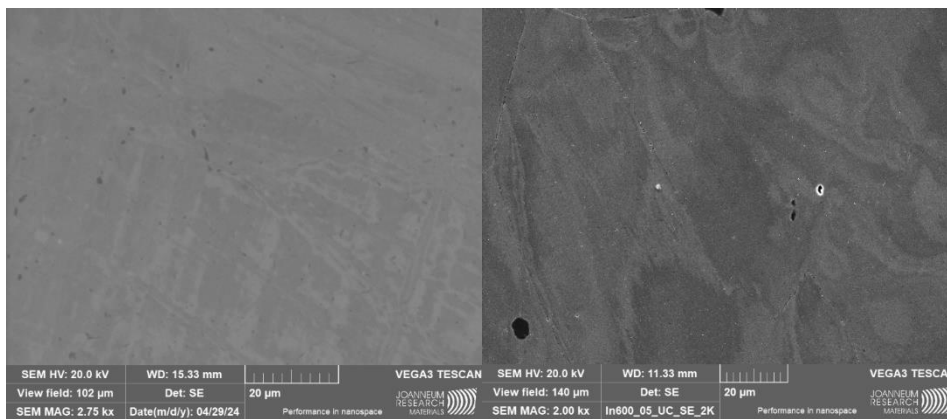


Figure 13: SEM images of different sections/samples to show the absence of the Hydrogen induced cracks and microstructural changes in HT charged samples (Sample 1).



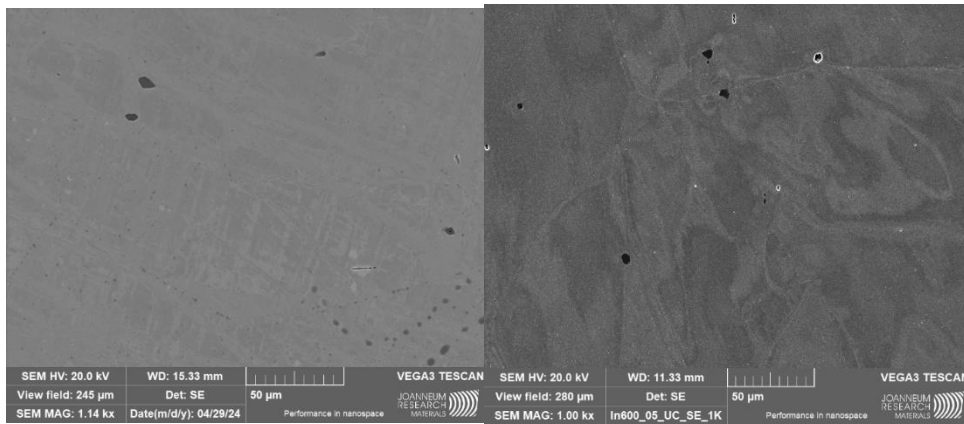


Figure 14: SEM images of different sections/samples to show the absence of the Hydrogen induced cracks and microstructural changes in HT charged samples (Sample 2)

**Material 2**

The following data shows the microstructural findings in the Material 2 alloy.

Table 15: Mass weight percentage of the uncharged, RT and HT Material 2; Sample 1

	Ni [%]	Cr [%]	W [%]	C [%]	Mo [%]	Fe [%]	Mn [%]
Uncharged	58.2	22.1	13.9	2.9	1.2	1.1	0.6
RT 48h	57.8	22.0	14.1	2.8	1.1	1.1	0.6
1000 °C 48h	58.5	22.5	11.8	n/c	1.1	1.1	0.6

Table 16: Atomic weight percentage of the uncharged, RT and HT Material 2; Sample 2

	Ni [%]	Cr [%]	W [%]	C [%]	Mo [%]	Fe [%]	Mn [%]
Uncharged	55.9	23.9	4.3	13.5	0.7	1.1	0.6
RT 48h	55.4	23.8	4.3	13.3	0.7	1.1	0.7
1000 °C 48h	62.2	27.0	4.0	n/a	0.7	1.2	0.7

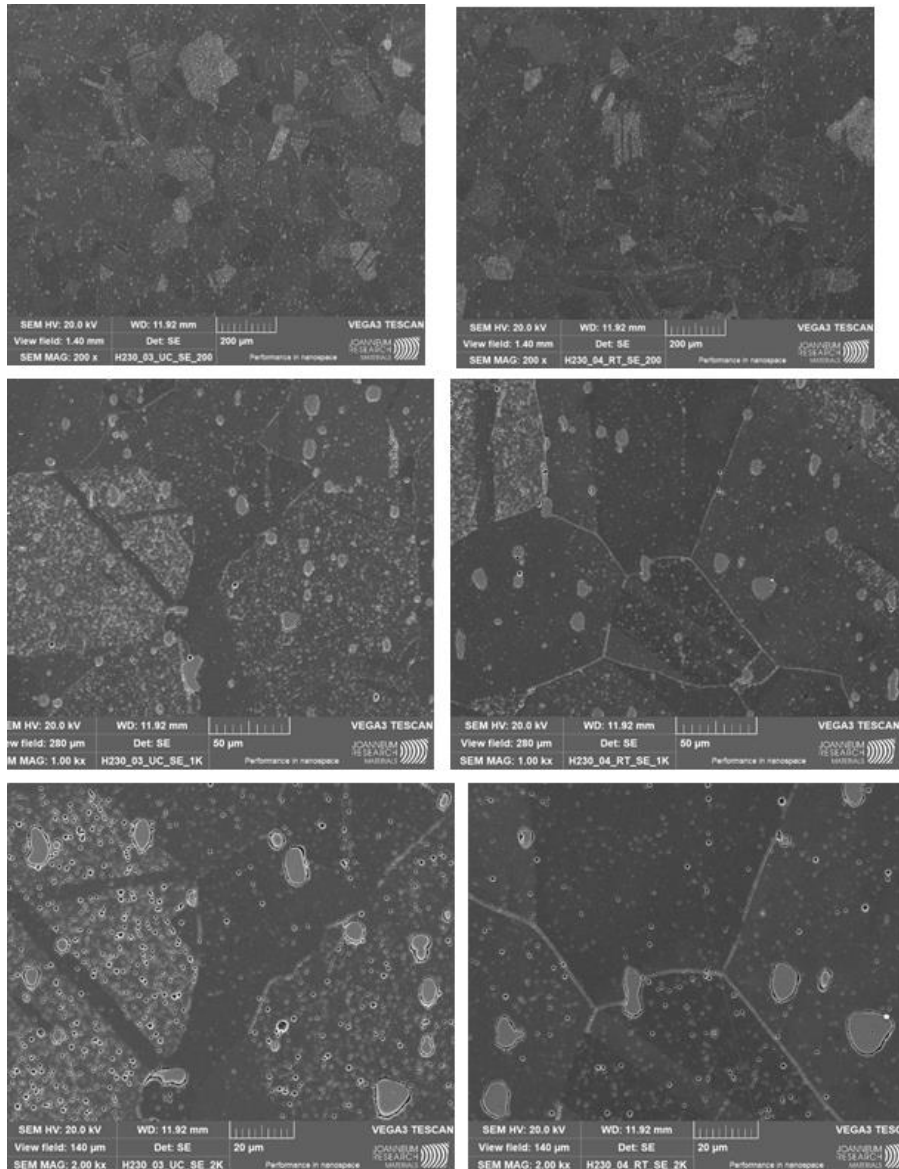


Figure 15. Microstructural analysis of the Material 2, sample 1 – left charged at RT, right uncharged, three different sections.

The grain size of the uncharged Haynes alloy varies from 50 – 200  $\mu\text{m}$ , whereas the number of grains above 200  $\mu\text{m}$  is relatively low. This phenomena does not change when charging the material with hydrogen. The FCC-matrix grains show quite well defined grain boundaries, as seen in figures below (*right uncharged and left charged 48 h*). Tungsten rich precipitates are evenly scattered throughout the material both in the uncharged and charged specimen. The precipitates and matrix grains do not change in size or deform during the process of hydrogenation. No crack or pores form through the charging process, which is in accordance with the fatigue behavior.

The specimen charged at elevated temperatures, above 1000  $^{\circ}\text{C}$ , also show no signs of hydrogen embrittlement within the SEM images. The grain sizes do not change evidently and more important no pores or additional inclusions can be found in the material. The SEM images below support the findings of the fatigue behavior.

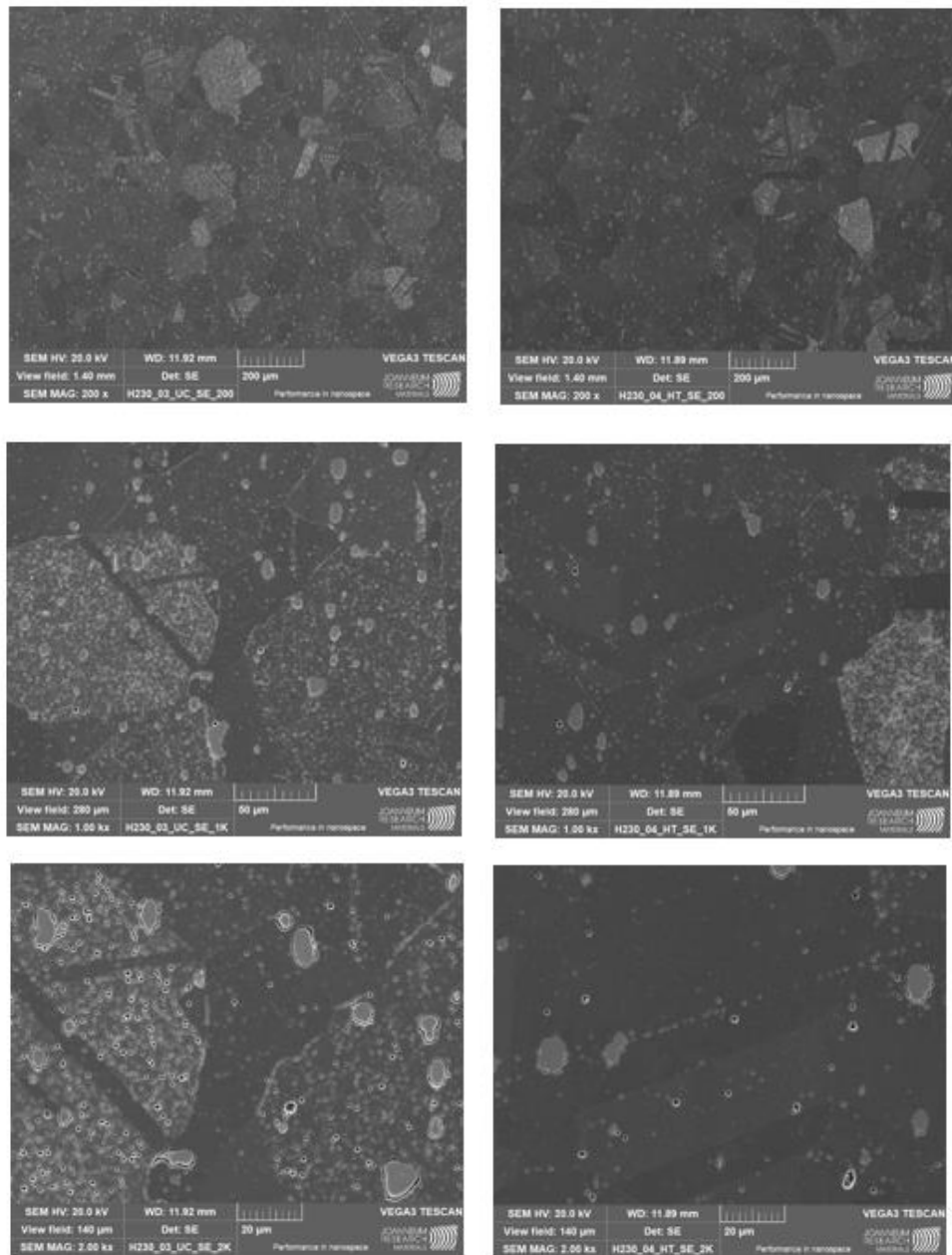


Figure 16. Microstructural analysis of the Material 2, sample 1 – left charged at HT, right uncharged, three different sections.

In form of a summary, three different charged samples were investigated using SEM analysis. Neither of the charged samples indicate cracks or pores induced by hydrogen, that is, other than already present in the uncharged sample. The hydrogen exposed specimen all show the same microstructural phases and no evidence of hydride formation was found via EDX analysis. Last but not the least, the mass percentage of the material does not change when charging with hydrogen – therefore we can conclude that no hydrides or other forms of inclusions have been formed throughout the process at room temperature and 1000 °C, as seen above.

#### 5.4.2 Fracture analysis

Although the fatigue machine doesn't commonly lead to the full fracture of the samples, and stops after the detection of the crack initiation in the sample, in determined samples the process was continued to the fracture on purpose. The aim was to make the fracture analysis and evaluation whether it could reveal any change in the fracture mode, which would denote the HE effects.

#### Material 1

The representative SEM fracture surfaces of Material 1 uncharged vs. 48 h charged at room temperature are presented in the figures below. The pictures represent the fracture surface after failure under maximum stress of 450 MPa.

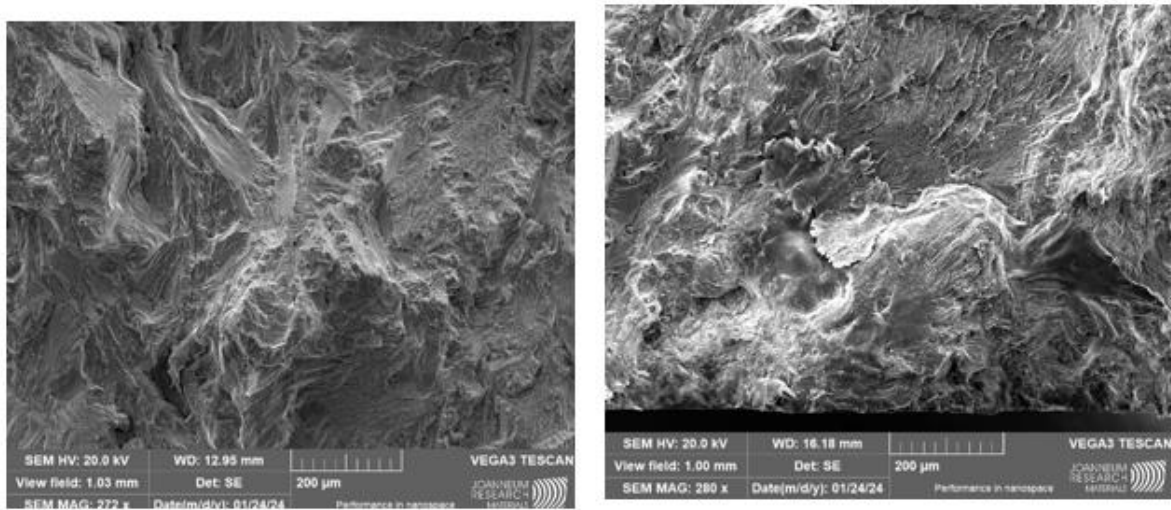


Figure 17: Fracture surfaces of Material 1 uncharged (right) vs. Material 1 charged at room temperature (left) outer region of sample

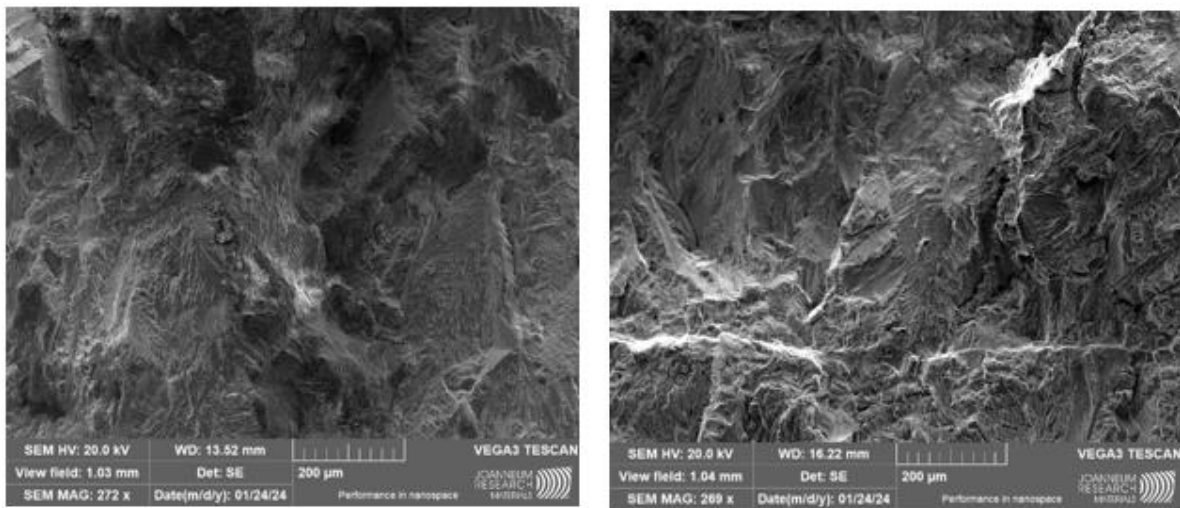


Figure 18: Fracture surfaces of Material 1 uncharged (right) vs. Material 1 charged at room temperature (left) outer region of sample

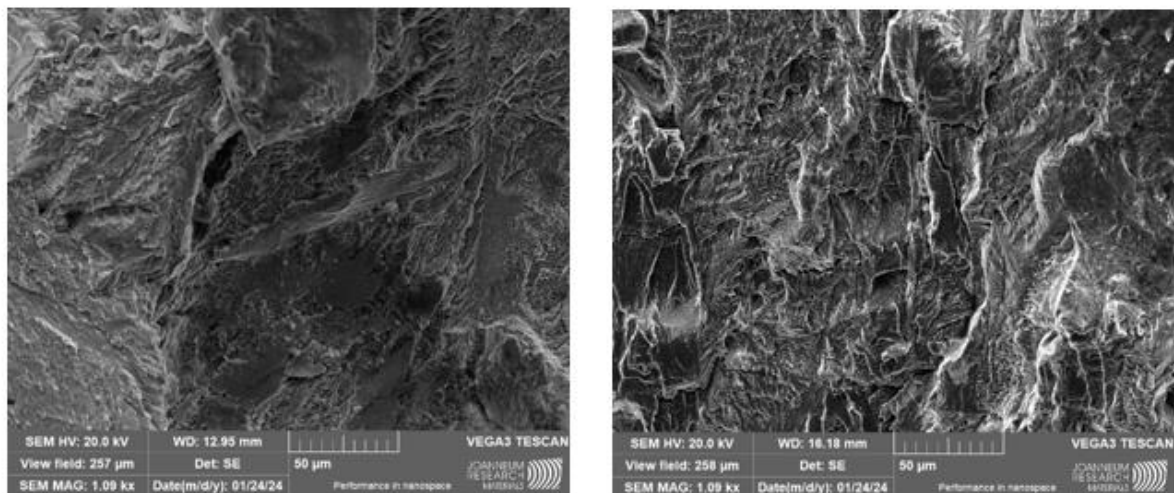


Figure 19: Fracture surfaces of Material 1 uncharged (right) vs. Material 1 charged at room temperature (left) inner region of sample

All non-hydrogen charged samples show a ductile breaking behaviour. In the inner region of the material, the specimen fractured via ductile micro-void coalescence, indicated by the dimples in this region. No transgranular facets are found in the non-hydrogen charged samples. The hydrogen charged samples display dimples within the inner region. The ductile behaviour of the fracture within the inner region of the material is due to the absence of hydrogen penetration in the bulk of the material. The outer region of the hydrogen charged specimen also display ductile behaviour as no transgranular facets or micro-facet cleavage can be found within the material, indicating an embrittlement of the material. *The absence of slip lines and tear ridges which are referenced to form through the hydrogen penetration<sup>16</sup>, cannot be found within this microstructure.*

Findings from the fracture surface analysis show that the hydrogen did not affect the fracture of the material and both non-hydrogen charged and hydrogen charged specimen show ductile behaviour indicated through the dimples throughout the material. This is also in accordance with the findings of the mechanical tests.

The representative SEM fracture surfaces of Material 1 uncharged vs. 48 h charged at high temperature are presented in the figures below. The pictures represent the fracture surface after failure under maximum stress of 450 MPa.

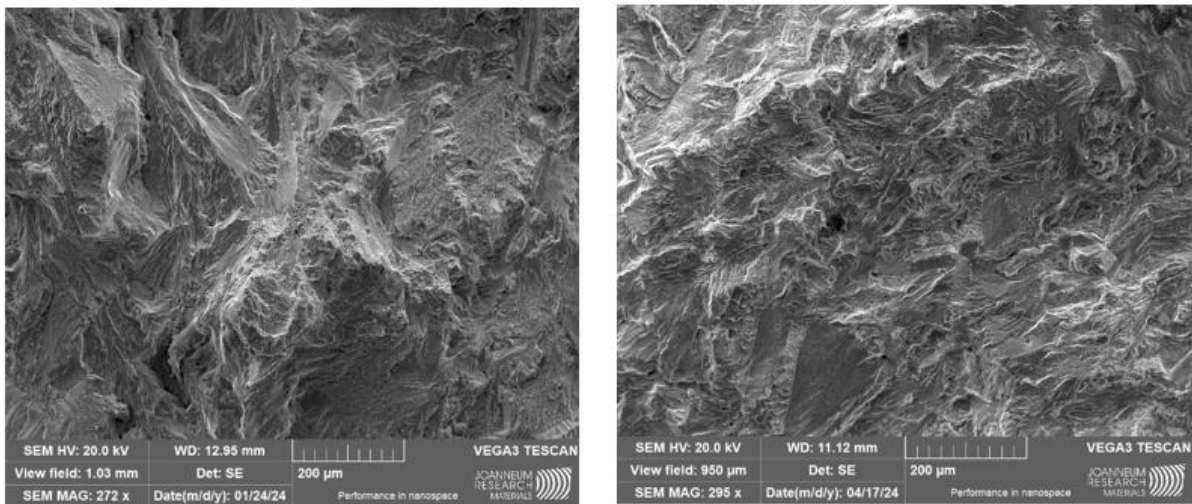


Figure 20: Fracture surfaces of Material 1 uncharged (right) vs. Material 1 charged at high temperature (left) outer region of sample

The fractography of Material 1 at high temperatures indicates that the material was not affected by hydrogen charging. The outer region of the sample indicate intergranular fractures, whereas the inner region of the material displays a more ductile fracture behaviour, as it shows more dimple like behaviour. Even though intergranular fractures can be found in the upper region of the material, where crack nucleation is initiated, this does not change from the uncharged to charged specimen and therefore we can conclude that at elevated temperature up to 1000°C the hydrogen does not brittle the Material 1 alloy.

<sup>16</sup> Acta Metallurgica Sinica (English Letters), 2020, 33(6): 759-773 DOI: 10.1007/s40195-020-01039-7

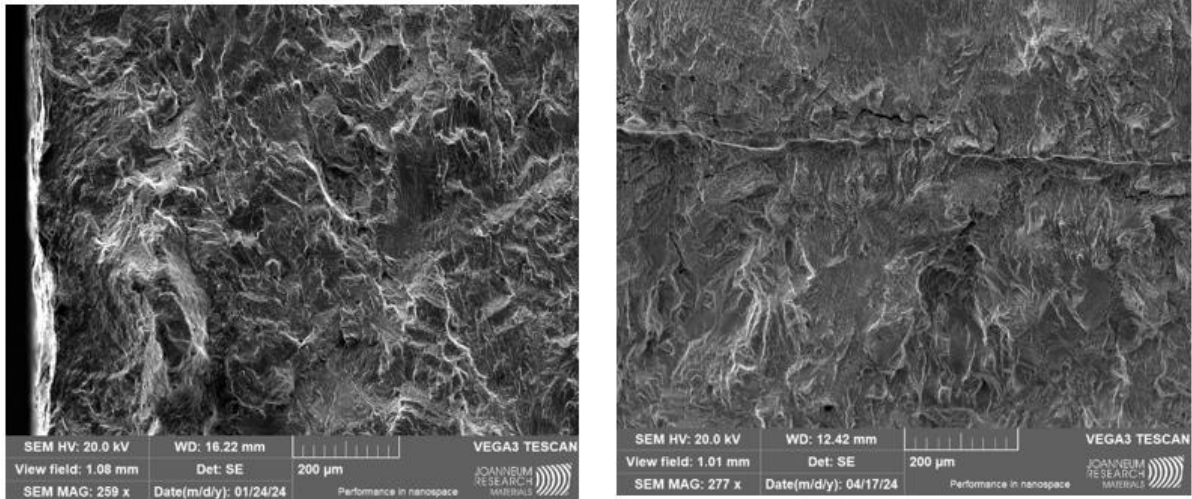


Figure 21: Fracture surfaces of Material 1 uncharged (right) vs. Material 1 charged at high temperature (left) outer region of sample

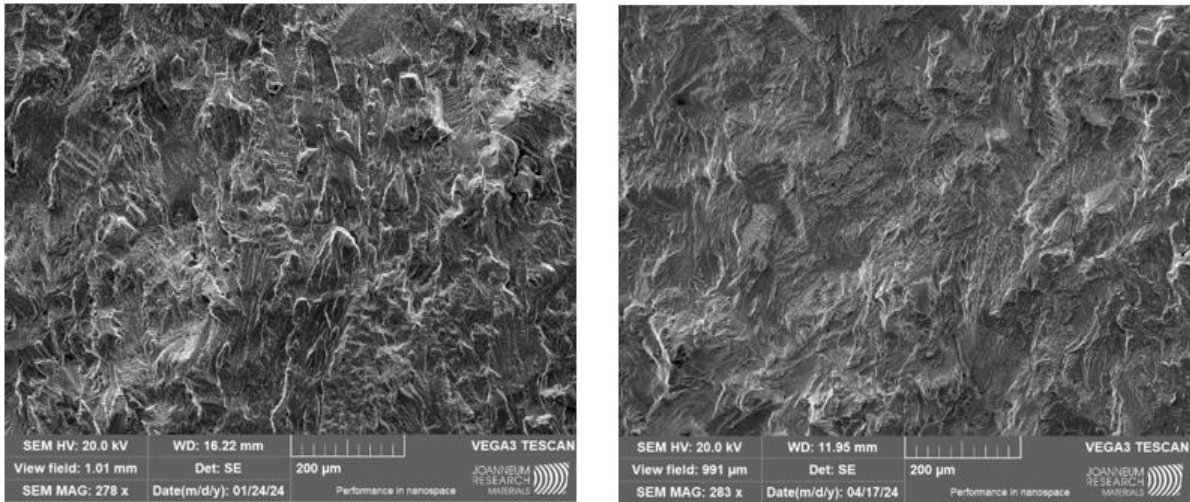
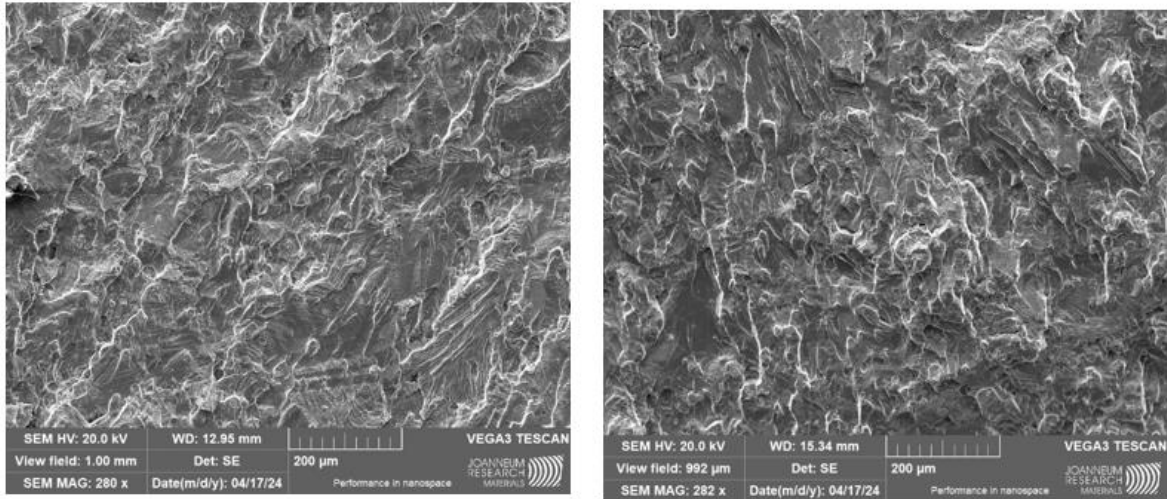


Figure 22: Fracture surfaces of Material 1 uncharged (right) vs. Material 1 charged at high temperature (left) inner region of sample

### Material 2

The representative SEM fracture surface of Material 2 uncharged vs. 48h charged at room temperature are represented in the figures below. The pictures represent the fracture surface after failure under maximum stress of 750 MPa.



*Figure 23: Fracture surfaces of Material 2 uncharged (left) vs. Material 2 charged at room temperature (right) inner region of sample*

The inner region of the uncharged and room temperature charged material show a very ductile fracture behaviour, due to the dimples, which have also already been explained for the Material 1 fracture behaviour.

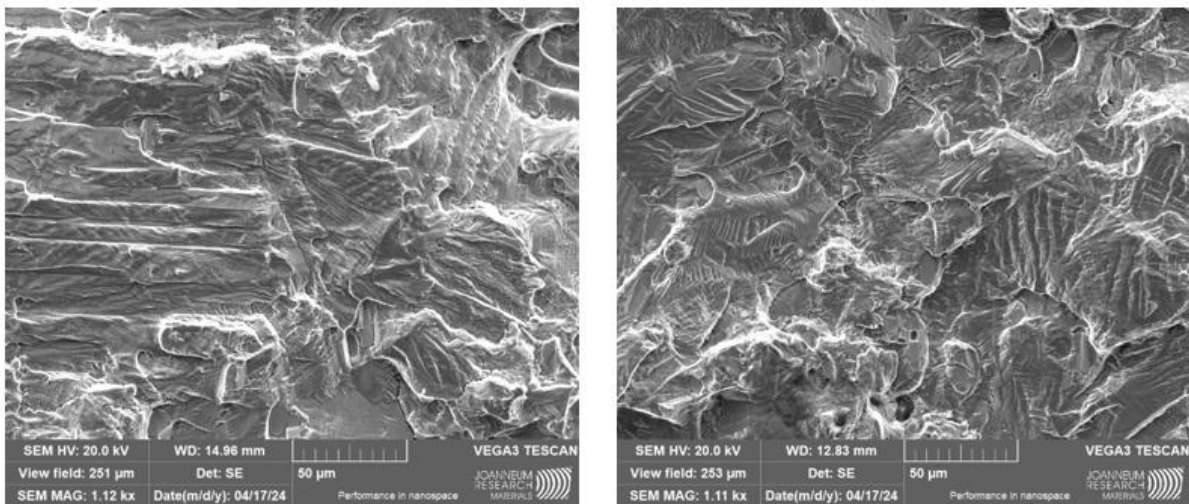


*Figure 24: Fracture surfaces of Material 2 uncharged (left) vs. Material 2 charged at room temperature (right) region of crack initiation of sample*

Within the upper part of the material, where the material starts breaking first, we can observe a more brittle behaviour, as we cannot find as many dimples as in the inner part of the material. But nonetheless, this is the same for the uncharged and charged material and therefore we can conclude that this is due to the breaking mechanism of the material and not caused by hydrogen embrittlement of the material.

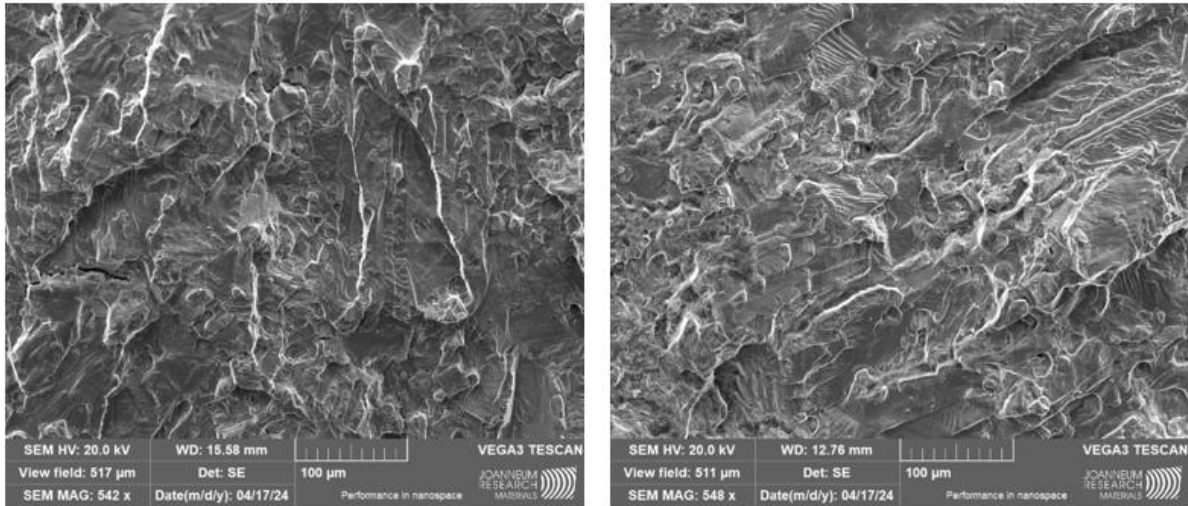


Figure 25: Fracture surfaces of Haynes uncharged (left) vs. Material 2 charged at room temperature (right) outer region of sample

No transgranular facets or micro-facet cleavage can be found in the outer or inner region of the material. Furthermore, the fracture behaviour of the 48h charged sample does not show any changes to the uncharged fracture which is a sign for no hydrogen embrittlement. If hydrogen molecules would have penetrated the material and caused damage, we would observe a brittle fracture, which is not the case.

Findings from the fracture surface analysis show that the hydrogen did not affect the fracture of the material and both non-hydrogen charged and hydrogen charged specimen show ductile behaviour indicated through the dimples throughout the material. This is also in accordance with the findings of the mechanical tests.

The representative SEM fracture surface of Material 2 uncharged vs. 48h charged at high temperature are represented in the figures below. The pictures represent the fracture surface after failure under maximum stress of 750 MPa.

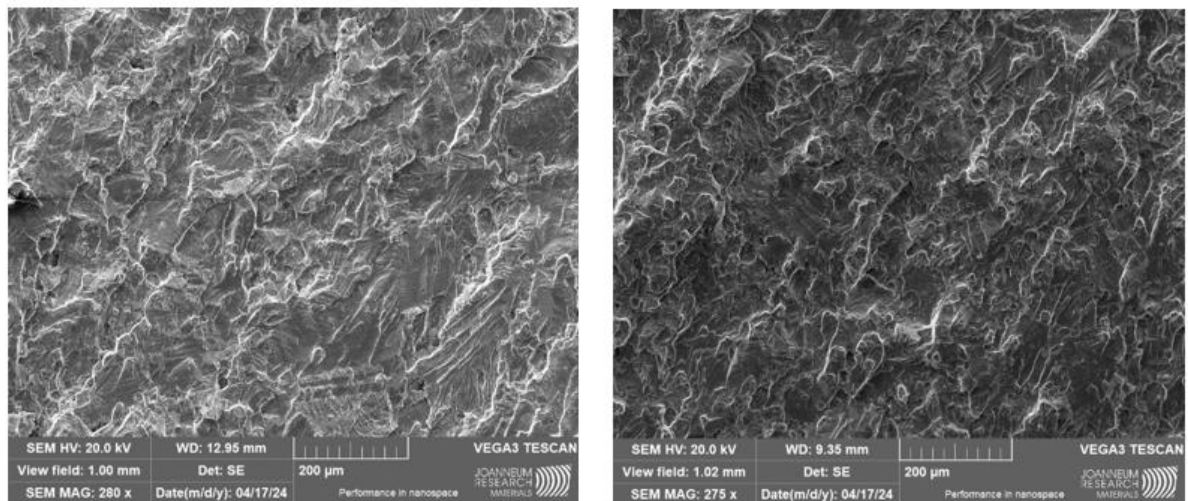


Figure 26: Fracture surfaces of Material 2 uncharged (left) vs. Material 2 charged at high temperature (right) inner region of sample

The inner region of the uncharged and high temperature charged material show a very ductile fracture behaviour, due to the dimples, which have also already been explained for the Material 1 fracture behaviour. Even though the temperature difference was increased by 1000 °C for charging, this did not change the fracture behaviour of the material in the inner region of the material. This means the hydrogen definitely did not affect the bulk of the material.

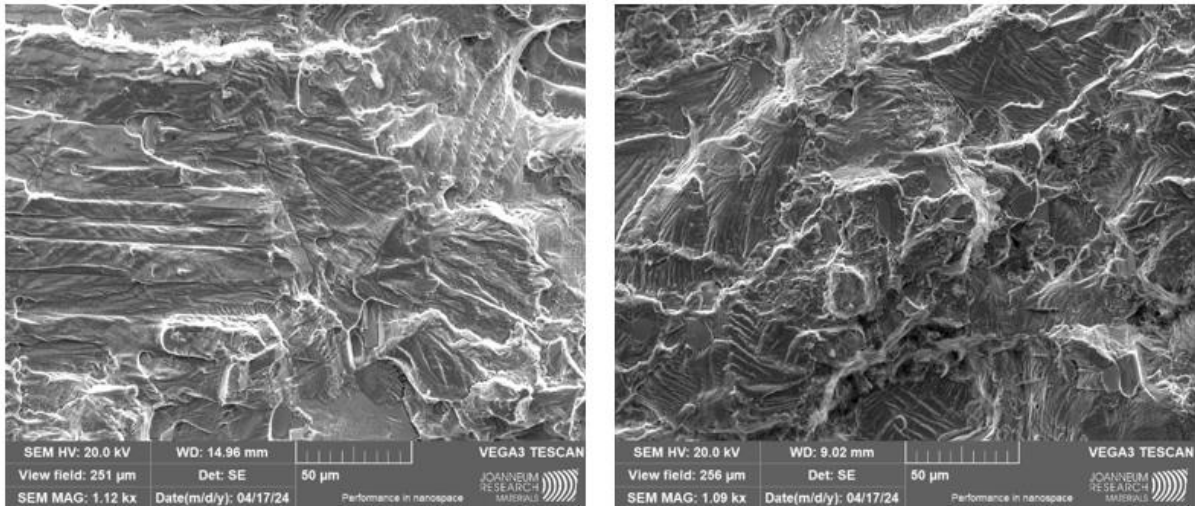


Figure 27: Fracture surfaces of Material 2 uncharged (left) vs. Material 2 charged at high temperature (right) region of crack initiation of sample

We can observe the same phenomena with the high temperature breakage as with the room temperature breakage, which is the following: Within the upper part of the material, where the material starts breaking first, we can observe a more brittle behaviour, as we cannot find as many dimples as in the inner part of the material. But nonetheless, this is the same for the uncharged and charged material and therefore we can conclude that this is due to the breaking mechanism of the material and not caused by hydrogen embrittlement of the material.

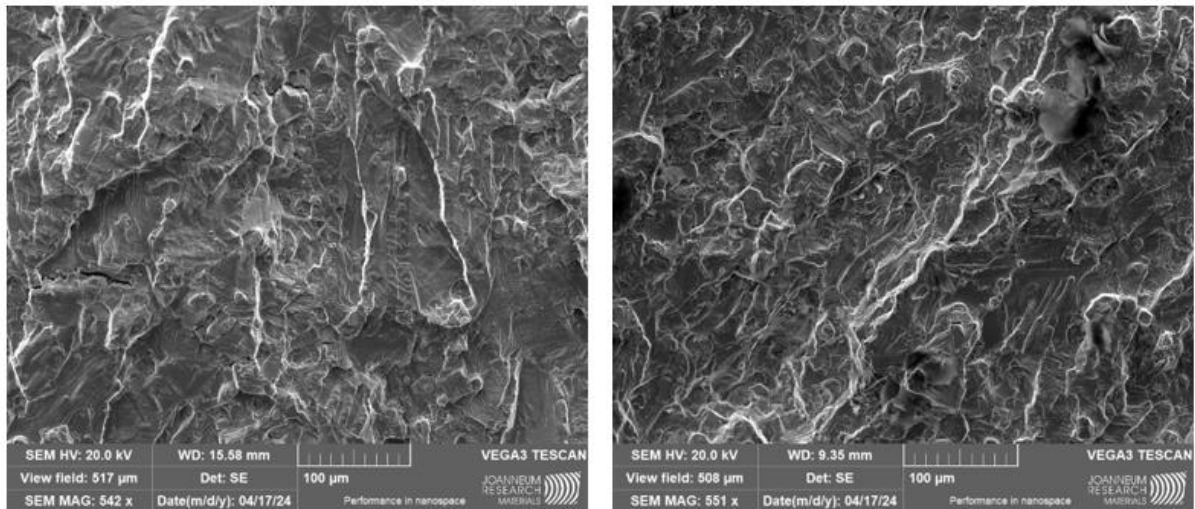


Figure 28: Fracture surfaces of Haynes uncharged (left) vs. Material 2 charged at high temperature (right) outer region of sample

The 48 h high temperature charged Material 2 Alloy does not show any difference in breakage/ fracture behaviour than the 48h room temperature material. The material overall shows a very ductile breaking behaviour and no changes in the SEM images indicate a change to a more brittle behaviour. Therefore, we can conclude that the hydrogen charging did not affect the fracture behaviour of the Material 2 Alloy.

## 6 Conclusions and future work

In the present report, we offer the results and discussion of the Hydrogen Embrittlement behaviour of materials that constitute the main components in the blast furnace fuel supply system.

The methodology was composed of mechanical test and microstructural analysis of the results. A novel approach to the hydrogen charging of material samples with Hydrogen gas has been developed and employed. After charging and testing, neither of materials showed relevant embrittlement and

microstructural change on both room and high temperature, which indicates their resistance to the phenomena of cracking or hydride formation.

It must be underlined that the charging was limited to 48h, which was the capacity of the consortium in this moment. Therefore, for future work, it is proposed that in the posterior stage of the project, once the project industrial facility is already installed and operation, the partners find a possibility to expose the samples to the real conditions, based on the real cycles of blast furnace usage with pure Hydrogen. This means, if the cycles are shown to be longer than 48h, that these time periods should be used for addition testing.